R. & M. No. 3211

R. & M. No. 3211

MINISTRY OF AVIATION

AERONAUTICAL RESEARCH COUNCIL
REPORTS AND MEMORANDA

An Experimental Investigation at Supersonic Speeds of the Characteristics of two Gothic Wings, one Plane and one Cambered

By L. C. Squire, Ph.D.

LONDON: HER MAJESTY'S STATIONERY OFFICE
1961
PRICE 14*s.* 0*d.* NET

An Experimental Investigation at Supersonic Speeds of the Characteristics of two Gothic Wings, one Plane and one Cambered

By L. C. Squire, Ph.D.

Communicated by the Deputy Controller Aircraft (Research and Development), Ministry of Aviation

Reports and Memoranda No. 3211

May, 1959

Summary. Tests have been made at supersonic speeds up to $M = 2 \cdot 0$ on a thick cambered gothic wing of aspect ratio $0 \cdot 75$, together with tests on the uncambered wing of the same plan-form and thickness. The camber was designed to give attached flow all along the leading edge, and over the whole wing, at one lift coefficient, together with low drag at this lift. The thickness distribution was chosen to have low zero-lift drag and also to eliminate the adverse pressure gradients due to incidence and camber at the design lift.

The results show that the drag of the cambered wing is close to the theoretically estimated value at the design lift coefficient: the drag of the plane wing, however, is also of the same magnitude and the reasons for this are discussed. Other properties of the wings are not in agreement with the slender thin wing theory. At the design condition on the cambered wing the flow is attached over the whole wing. Off-the-design condition the leading edge separations on the cambered wing are much weaker than on the plane wing.

1. *Introduction.* In connection with the design of slender wings of high lift/drag ratios a considerable amount of theoretical work has been directed to determining area distributions with low zero-lift drag[1]; much effort has also been given to producing cambered surfaces on slender, curved edged, plan-forms with attached flow at the leading edge at a positive lift, together with low drag at this lift[2,3]. The drag was calculated by slender-body theory and the camber designed by slender-thin-wing theory, since there is no more appropriate theory available for wings with curved leading edges. Experimental work in progress is confirming, in most cases, the theoretical zero-lift wave drag, but experimental results on some thin cambered wings are disappointing in that although the flow is attached at the leading edge at the design lift coefficient, the boundary layer separates elsewhere on the wing and so causes much higher drag due to lift than predicted. Further work has suggested that adverse pressure distributions on the thin cambered wings can be overcome by suitable combinations of thickness and camber[4].

Previously issued as R.A.E. Tech. Note Aero. 2620—A.R.C. 21,390.

In this note test results, obtained in the 3 ft Tunnel at the Royal Aircraft Establishment, Bedford, on a cambered wing incorporating these features are described, together with the test results on the uncambered, or plane wing of the same thickness. Both wings have gothic plan-forms.

The basis of the design of these wings is described in Section 2, but it should be emphasised that the object of the tests was to check the theory, rather than to produce, and test, an optimum wing. Thus the wings tested are rather thick (8·2 per cent on the centre-line) to reduce the relative magnitude of the sting distortion interference and also to ease model manufacture.

In addition to checking the design methods, the tests provide data on the characteristics of a gothic plan-form at supersonic speeds and also on those of a cambered wing at off-design conditions.

2. *Reasons for the Choice of Models.* When it was decided to test thick cambered wings in the 3 ft Tunnel a study of some of the possible combinations of thickness and camber was made to decide the most suitable configuration*. An outline of these considerations is given here since the calculated properties of the wings are relevant to the analysis of the experimental results; also they may be useful in the extrapolation of the results to full-scale conditions, possibly with different thickness distributions and camber design lift coefficients.

The gothic plan-form of aspect ratio 0·75 was chosen since there were very few high-speed tests planned on this shape and so the plane wing, in addition to providing the basic data to compare with the cambered results, would also give high-speed data on the gothic plan-form. The aspect ratio was such that within the tunnel speed range (up to $M = 2{\cdot}0$) the slenderness parameter, $(s/c_0)\beta$, varied from 0·25 at $M = 1{\cdot}4$ to 0·43 at $M = 2{\cdot}0$, this higher value being near the possible limit for the application of slender-wing theory.

A model of 20 in. root chord with this plan-form necessitated a circular body of 1·35 in. in diameter at the rear of the model to shield the strain-gauge balance and support sting (*see* Fig. 1). To keep the interference of this distortion small it was necessary to make the wing relatively thick.

The choice then reduced to the addition of thickness to the camber design to give a suitable thick cambered wing which had a reasonable lift/drag ratio, allowed accurate measurement of drag due to lift both below and above design lift and also had a pressure distribution, found by the addition of the pressures due to thickness and camber, such that separations were unlikely to occur except at the leading edge in off-design conditions. Since the wing had to be fairly thick a 'Lord V' area distribution[1] was chosen since it has a low drag and also a favourable pressure gradient over the whole wing. Diamond cross-sections were chosen to ease model manufacture. The drag and wing size were fixed by choosing the wing volume as $0{\cdot}009c_0^3$. This wing volume resulted in a wing of 8·2 per cent thickness/chord ratio on the centre-line. The wave drag coefficient according to slender-body theory varied from 0·0082 at $M = 1{\cdot}4$ to 0·0072 at $M = 2{\cdot}0$. The theoretical pressure distributions on the uncambered wing are shown in Fig. 4.

The camber was then chosen from some examples calculated by Weber in Ref. 2; in fact Wing 4 of that report. This wing is uncambered inboard of a line joining the apex to a point 80 per cent out along the trailing edge (Fig. 2). Outboard of this line the downwash distribution is parabolic. At the design lift coefficient the drag due to lift, as given by not-so-slender wing theory, is—

$$C_D = \frac{1}{\pi A}\left\{1{\cdot}07 + \left(\frac{\beta s}{c_0}\right)^2\left(1{\cdot}88 - 0{\cdot}06\log\frac{\beta s}{c_0}\right)\right\} C_L{}^2.$$

* The design of thick cambered wings is more fully discussed by Maskell and Weber[4]; their examples are related to the wings described in this Note.

The pressure distributions on this thin wing are shown in Fig. 5. It will be seen that the gradient is unfavourable over most of the wing; however, with a design lift coefficient of 0·1 these adverse gradients are almost eliminated by the addition of thickness (Fig. 6)*.

A lower drag due to lift could have been obtained by only cambering the wing outboard of a line joining the apex and wing tip. However, the wing shapes in this case were very extreme near the leading edge and it was felt that these sharp changes might invalidate the theory as well as making the model manufacture almost impossible.

The theoretical properties of the two wings are given in Table 1.

3. *Details of the Tests.* 3.1. *Description of the Models.* Fig. 1 shows details of the plane wing. This wing was made of steel and had a small circular section body at the back to shield the strain-gauge balance and the support sting.

Details of the cambered wing are given in Figs. 2 and 3. Fig. 2 shows the wing plan-form and camber region together with a side view of the leading edge. Spanwise sections at various positions along the chord are shown in Fig. 3. It should be noted that the thickness was added to the camber surface so that the area of spanwise sections, and hence the wing volume, were the same for both the plane and cambered wings. (This means that the thickness was *not* added normal to the cambered surface.) This method of adding thickness is illustrated in Fig. 3.

The cambered wing was made of laminated glass-cloth and Araldite formed onto a steel core which was used to attach the model to the balance. The sting shield was made of steel, integral with this core, and was similar to that of the plane wing.

Full dimensions of both models are given in Table 2.

The leading edge of the plane steel wing was approximately 0·002 in. thick and the wing thickness was within 0·0025 in. of the correct value. The cambered wing was less accurate and the leading edge was approximately 0·005 in. thick.

3.2. *Experimental Details.* Measurements of lift, drag and pitching moment were made in the 3 ft Supersonic Tunnel at Mach numbers of 1·42, 1·61, 1·82 and 2·00 through an incidence† range of − 4 deg to + 10 deg in one degree steps. The Reynolds number was kept constant at 2×10^6 based on the aerodynamic mean chord of 15 in. This Reynolds number corresponded to a tunnel total pressure of just under half an atmosphere. This low total pressure was dictated by the low strength of the Araldite model. It had been planned to test the steel plane model up to a Reynolds number of $4{\cdot}5 \times 10^6$, but during the period of the tests tunnel power was limited so that these high Reynolds number tests were not made. Instead, in an attempt to assess Reynolds number effects tests on both models were made with transition fixed and free. Transition was fixed by a band of carborundum in aluminium paint along the leading edge on both surfaces. This band was 1 in. wide at the wing centre-line (5 per cent of the chord) and varied smoothly to a band 0·5 in. wide at the tip (*see* Fig. 1). Sublimation tests showed that at zero incidence at $M = 2{\cdot}0$ the flow was laminar over the whole wing with no roughness band, but that the carborundum fixed transition at the band.

---

* The pressure distributions on the thick cambered wings are obtained by adding the velocities due to thickness and camber.

† Incidence of the cambered wing refers to the incidence of the uncambered centre section.

Surface oil-flow observations were also made at various incidences at $M = 1{\cdot}61$ for both wings. The patterns on the plane wing were obtained in the transition-free case since the main interest on this wing was in the leading-edge flow. On the cambered wing oil patterns were obtained in both the transition-free and fixed cases.

3.3. *Reduction and Accuracy of Results.* The balance results have been reduced to the usual coefficient forms; for both wings the reference areas and chords are based on the plane wing plan-form. The pitching-moment coefficients are referred to the quarter-chord point of the mean aerodynamic chord. The drag has been corrected to a base pressure, at the body base, equal to free-stream static.

From a consideration of the possible sources of error, together with a study of repeat readings it is believed that the accuracy of the results is as follows:—

C_L	$\pm 0{\cdot}003$
C_m	$\pm 0{\cdot}0005$
C_D	$\pm 0{\cdot}0004$ at $C_L = 0$
	$\pm 0{\cdot}001$ at $C_L = 0{\cdot}3$
α	$\pm 0{\cdot}05°$

These limits are overall values, and the relative accuracy of results from consecutive incidences is probably much better than this.

4. *Discussion of Results.* 4.1. *Presentation of Results.* The measured coefficients are tabulated in Tables 3 and 4. The coefficients for the plane wing are plotted in Figs. 7 to 10 (C_L against α, C_m against C_L, C_D against C_L and C_L^2) for the four Mach numbers with transition free and fixed. The corresponding results for the cambered wing are presented in Figs. 11 to 13 (no plot of C_D against C_L^2). Oil flow patterns for the plane wing (transition free) are given in Fig. 14 and for the cambered wing in Figs. 15, 16 and 17. The lift/drag ratios of the two wings are compared in Figs. 18 and 19. The remaining figures present various derived data, and these figures will be referred to in the following analysis as necessary.

Before a full discussion of the results it is worth noting some features of the lift/drag ratios in Figs. 18 and 19. At low lift the plane wing has the higher lift/drag ratio, but with increase in lift the cambered wing tends to gain a slight advantage; however, at lift coefficients near $0{\cdot}1$ the lift/drag ratios of both wings are very similar. At $C_L = 0{\cdot}1$ the ratios for both wings (transition fixed) are very close to the estimated value for the cambered wing (Table 1). The discussion of the results therefore can be conveniently divided into three parts: discussion of the plane wing results and of why its lift/drag ratio is higher than expected*, discussion of the cambered wing results and thirdly a comparison of the two wings.

* Prior to these tests it had been assumed that the factor K in the drag due to lift ($KC_L^2/\pi A$) of the plane gothic wing would be lower than 2, because of leading edge vortex formation, but that the amount below, at $C_L = 0{\cdot}1$, would not be much. If this were the case the lift/drag ratio of the plane wing, transition fixed, would be expected to be about $4{\cdot}2$ at $C_L = 0{\cdot}1$ compared with approximately $4{\cdot}8$ (Table 1) for the cambered wing, since the camber was designed to give a much lower drag due to lift.

4.2. *Plane Wing Results.* In both the curves of C_L plotted against α and C_m against C_L, Figs. 7 and 8, non-linear effects are apparent at non-zero lift. In the lift curves at $M = 1{\cdot}42$ and $1{\cdot}61$ in particular the non-linear effects begin at one degree (i.e. $C_L < 0{\cdot}03$), if not lower. These effects are independent of transition fixing, suggesting that they are caused by leading edge separations. This is confirmed by the oil flow patterns on the suction side of the wing at $M = 1{\cdot}61$ in Fig. 14. At 1 deg incidence the oil pattern is clearest on the starboard wing. There is a separation line just inboard of the leading edge along most of the chord; inboard of this separation can be seen the characteristic spiral pattern of a rolled-up vortex sheet. At 4 deg incidence the separation line has moved inboard and the region of spiral pattern has increased in size. Thus a vortex appears to lie along most of the leading edge at 1 deg incidence. This vortex moves inboard and increases in strength with increasing incidence.

As the Mach number is increased the non-linear lift is less apparent at the lower incidences. It is believed that this is due to a region of attached flow at the apex of the wing at low incidence, since at a free-stream Mach number of $M = 2{\cdot}0$, the component normal to the leading edge at the apex is $0{\cdot}9$, and this normal component has been found, on delta wings[5], to give attached flow at the lower incidences. It was not possible to check this idea by oil flow visualization since the tunnel starting loads at $M = 2{\cdot}0$ produced violent sting vibrations which limited the number of runs at this speed. However, a more rigid sting is being manufactured and these oil flow tests will be made later.

The upper-surface separations also cause a stabilising movement of the centre of pressure with incidence. At $M = 1{\cdot}61$, for example, the centre of pressure on the transition-fixed wing moves from 42% $\bar{\bar{c}}$ at $C_L = 0$ to 45% $\bar{\bar{c}}$ at $C_L = 0{\cdot}3$ (the corresponding figures with transition free are 41% $\bar{\bar{c}}$ to 45% $\bar{\bar{c}}$). Results for other Mach numbers are compared with the cambered results in Figs. 22 and 23.

Another marked feature of the lift curves is that even at zero incidence their slopes are much higher than the theoretical values given by slender-wing theory. These results are plotted in Fig. 20, where it will be seen that $(\partial C_L/\partial\alpha)$ varies from $1{\cdot}45$ per radian at $M = 1{\cdot}42$ to $1{\cdot}30$ at $M = 2{\cdot}00$, compared with the slender-wing value of $1{\cdot}18$ per radian. The experimental values are independent of transition fixing. Also plotted in Fig. 20 is the linear-theory lift-curve slope for a cropped delta of the same aspect ratio and span/chord as the gothic wing[6]. It will be seen that the agreement in this case is very good.

The values of $(\partial C_m/\partial C_L)$ presented in Fig. 21 again show that the experimental results do not agree with the slender-wing values. In this case the aerodynamic centre by slender-wing theory is at $29{\cdot}9\%$ $\bar{\bar{c}}$, whereas the experimental values, again almost independent of transition fixing, vary between $42{\cdot}5\%$ $\bar{\bar{c}}$ at $M = 1{\cdot}42$ to $44{\cdot}5\%$ $\bar{\bar{c}}$ at $M = 2{\cdot}00$. The linear-theory values for the cropped delta, transferred to the aerodynamic mean chord of the gothic, vary between $32{\cdot}5\%$ $\bar{\bar{c}}$ at $M = 1{\cdot}42$ to 38% $\bar{\bar{c}}$ at $M = 2{\cdot}00$.

Considering now the drag results; the basic curves of C_D against C_L and C_L^2 are presented in Figs. 9 and 10. The variation of $(C_D)_0$ with Mach number is shown in Fig. 24 and the variation of the drag due to lift factor with Mach number and lift in Fig. 25. The main point of interest in the C_D vs. C_L (Fig. 9) curves is the dip in drag at zero lift at $M = 1{\cdot}42$ when transition is free. This sudden increase in drag, with small increase in incidence, from the zero incidence value is thought to be caused by the forward movement of the transition position giving increased skin friction in the lifting condition. The plots of C_D against C_L^2 show that C_D varies linearly with C_L^2 right up to

the highest lift tested, except at the lower lifts at $M = 1{\cdot}42$ and $1{\cdot}61$, transition free, where the non-linear variations are probably due to the changes in transition position noted above.

Fig. 24 also shows the estimated values of $(C_D)_0$ from Table 1. It will be seen that with transition fixed the experimental results* are about $0{\cdot}0007$ below the estimated values, whereas for the transition-free case the experimental points are $0{\cdot}0015$ below the estimate at $M = 1{\cdot}42$ and $0{\cdot}0003$ above at $M = 2{\cdot}00$. Although the trend of the variation of the transition-fixed results agrees with that of the theoretical values the difference in level corresponds to about 10 per cent of the estimated wave drag. This lower experimental drag could be partly due to the interference of the sting body, which appears likely to decrease the drag. In addition it must be noted that skin friction and wave drag make almost equal contributions to the estimated overall drag, and so over estimation of the skin friction could account for some of the apparent higher estimated drag.

The 'lift-dependent drag factor', $\pi A(C_D - C_{D0})/C_L^2$, is plotted against C_L in Fig. 25 for the four test Mach numbers. Only the transition-fixed experimental points are given in the Figure; the transition-free results are not included since changes in transition position made interpretation of the results difficult. The chain-dotted curve represents the lift-dependent drag factor given by not-so-slender body theory[2,7]. The dotted curve is the experimental variation of $\pi A(C_{L\alpha})/C_L^2$; this is the lift-dependent drag factor if the measured loading on the wing due to incidence is assumed to act normal to the wing chord plane, i.e. it is the case with no leading edge suction and no thickness. It will be seen that above $C_L = 0{\cdot}1$ the factor $\pi A(C_D - C_{D0})/C_L^2$ is almost independent of C_L and lies just above the not-so-slender value except at $M = 1{\cdot}82$ where, for reasons not yet understood, it agrees with the not-so-slender value. At lower lift the drag due to lift is well below the no-suction flat plate value. It is thought that the lower values at the lower lift coefficients are caused by the separation vortices producing a suction inboard of the leading edge. These suctions would tend to reduce the axial force and hence have a favourable effect on drag.

At this stage it appears possible to explain the low drag of the plane wing as due to two causes. Firstly, the lift-curve slope of the gothic plan-form, even near zero incidence in the absence of leading edge separations, is much higher than slender-wing theory predicts, so that the lift-dependent drag factor is lower than the value of 2 given, in the absence of leading edge suction, by slender-wing theory. Secondly, the lift-dependent drag is reduced by the leading edge separation vortices which further decrease the incidence for a given lift and also combine with the wing thickness to produce a favourable axial force.

The higher lift-curve slope is predicted by linear theory for a related cropped delta wing, and probably linear theory for the gothic wing would also predict this higher lift. The failure of slender-wing theory for these plan-forms at the relatively low values of the slenderness parameter may be explained by the fact that in slender-wing theory the lift at any point on an uncambered wing depends only on the leading edge sweep at the same chord-wise position as the point where the lift is to be found: thus the (slender wing) lift falls to zero at the trailing edge of the gothic wing, and is also small over the whole of the rear of the wing. In linear theory, on the other hand, the lift depends on the whole of the leading edge in the upstream Mach cone of the point, and so need not be small near the trailing edge. Thus it might be supposed that slender-wing theory would predict a low lift acting too close to the nose.

* At $M = 1{\cdot}42$ the experimental point is plotted $0{\cdot}0006$ below the tabulated value. This is because the test at this Mach number was made at a Reynolds number of $1{\cdot}4 \times 10^6$ instead of 2×10^6 due to a cut in power. $0{\cdot}0006$ represents the estimated increase in skin friction due to the lower Reynolds number.

4.3. *Cambered Wing Results.* The variations of C_L with α and of C_m with C_L are plotted in Figs. 11 and 12. It will be seen that the lift curve is linear throughout the incidence range, while the moment curve shows a slight increase in stability with increased lift, these observations being true for the wing with and without fixed transition. The lift-curve slopes plotted in Fig. 20 are about 15 per cent higher than the zero-lift slopes for the plane wing. Smith, in some work on cambered delta wings[8] has shown that the lift-curve slope for a cambered surface will be greater than for the uncambered wing; thus Smith's theory and experiment are consistent in this respect.

It is interesting to note that at all Mach numbers the C_L of $0{\cdot}1$ occurs between 5 deg and $5{\cdot}5$ deg incidence, compared with the design value of $5{\cdot}5$ deg.

The change in centre of pressure with lift, Figs. 22 and 23, is generally less above $C_L = 0{\cdot}1$ than that on the plane wing. At $C_L = 0{\cdot}1$ the centre of pressure moves back from $42{\cdot}5\%$ $\bar{c}$ at $M = 1{\cdot}42$ to 45% $\bar{c}$ at $M = 2{\cdot}0$, compared with the slender-wing position of 36% $\bar{c}$ for all Mach numbers.

Some oil flow patterns for the cambered wing are shown in Figs. 15 and 16; these show the oil patterns at lift coefficients of approximately $0{\cdot}1$ and $0{\cdot}2$. It was difficult to get clear oil patterns on the Araldite surface of the cambered wing, but these photographs show the type of flow which occurred. Deductions from these, and other flow patterns, are summarised in Fig. 17 and will be described in the following paragraphs.

At the design C_L, Fig. 15, the flow is attached over the whole wing, except possibly at the extreme tip on the upper surface where there is a large drop of oil. At $C_L = 0{\cdot}198$, Fig. 16, there is a leading edge separation which appears to start at about 40 per cent of the leading edge from the nose, and which rolls up into a vortex lying along the highly drooped leading edge. This vortex is close to the edge (Fig. 17) and cannot have a large effect on lift. Inboard of the leading edge, near the shoulder position, there is a marked convergence of the oil streamlines over the rear 20 per cent of the wing. It is difficult to decide whether this is a local region of separation, or just a sharp change in flow direction due to the rapid change of surface shape in this region. When transition is fixed the convergence is less marked and it is believed that there may be a thickening of the boundary layer in this region.

Oil patterns at $C_L = 0{\cdot}138$ (approximately 1 deg above design) showed no sign of any separation on the wing except at the extreme tips. Below the design lift, at $C_L = 0{\cdot}048$ there was a very small separation along most of the leading edge on the under surface. At $C_L = -0{\cdot}40$ this separation had moved forward and increased in strength but was still well within the drooped leading edge (Fig. 17). These separations appear to have no influence on the wing lift, but act to give an unfavourable effect on drag.

The drag variation with C_L is plotted in Fig. 13 and the lift dependent drag factor (transition fixed) with C_L in Fig. 26.

For convenience in analysis this lift dependent drag factor has been based on the difference between the drag of the cambered wing and a drag equal to the experimental zero-lift drag of the plane wing together with an increment of $0{\cdot}0007$ to allow for the difference of skin friction for the cambered wing. At negative lift the lift dependent drag is much higher than at positive lift; in both cases it is very large at low lift. At $C_L = 0{\cdot}1$, the design lift coefficient, the drag factor is always higher than the theoretical value, being nearest to the theoretical at $M = 1{\cdot}82$ where it is $1{\cdot}48$ compared with the theoretical value of $1{\cdot}34$. At all Mach numbers the lift-dependent drag factor falls with increasing lift and is always below the design theoretical value above $C_L = 0{\cdot}2$.

Compared with the plane wing which has a lift-dependent drag factor which is almost independent of C_L the cambered wing has more drag due to lift at $C_L = 0{\cdot}1$, but less at $C_L = 0{\cdot}2$.

At this stage the properties of the cambered wing as compared with theory can be reviewed.

(*a*) The lift-curve slope of the cambered wing (and also of the plane wing) is much higher than the corresponding slende.. wing theory value.

(*b*) The centre of pressure of the cambered wing at design is between $6{\cdot}5\%$ $\bar{c}$ to 9% $\bar{c}$ behind the theoretical value in the speed range from $M = 1{\cdot}4$ to $M = 2{\cdot}0$.

(*c*) The design lift coefficient of $0{\cdot}1$ is obtained at an incidence within $0{\cdot}5$ deg of the theoretical value ($5{\cdot}5$ deg).

(*d*) The drag due to lift at the design lift coefficient of $0{\cdot}1$ is higher than the theoretical value by about 10 per cent, but drops below this value above lift coefficients of $0{\cdot}2$.

In Section 4.2 it has already been noted that slender-wing theory appears inadequate for the gothic plan-form and these comparisons tend to confirm this failure.

4.4. *Comparison of the Two Wings.* During the analysis of the results for the plane and cambered wings various comparisons between the two wings have been made. In this Section these comparisons will be briefly reviewed, and some additional points made.

The centres of pressure of the two wings are shown in Figs. 22 and 23. In general, at positive C_L, the cambered-wing centre of pressure is 2% $\bar{c}$ in front of that of the plane wing at $M = 1{\cdot}42$, but by $M = 2{\cdot}0$ the centres of pressure of the two wings are together.

The L/D ratios at $C_L = 0{\cdot}1$ are compared in Fig. 27, while maximum values of L/D are compared in Fig. 28 and the C_L's for these maximum values in Fig. 29. For the transition-fixed case the plane wing has the higher L/D at $C_L = 0{\cdot}1$, whereas the maximum values are almost the same for both wings, although the maximum for the cambered wing occurs at $0{\cdot}02$ C_L higher than for the plane wing. These comparisons, however, apply only at the test Reynolds number; increase in Reynolds number will increase the maximum L/D and lower the C_L at which it occurs. These changes would be greater on the cambered wing due to its larger wetted area. The results for the transition-free case are, in general, consistent with the transition-fixed results but full comparisons are difficult because of varying transition effects.

Finally, the lift at various incidences is compared in Fig. 30. This Figure shows that at zero incidence the cambered wing has a negative lift which varies from $C_L = -0{\cdot}05$ at $M = 1{\cdot}42$ to $-0{\cdot}04$ at $M = 2{\cdot}0$. This lower lift of the cambered wing continues at all incidences, for example at 8 deg the difference is $0{\cdot}066$ at $M = 1{\cdot}42$ and $0{\cdot}04$ at $M = 2{\cdot}0$.

5. *Conclusions.* Tests, at supersonic speeds up to $M = 2{\cdot}0$, have been made on a thick cambered wing designed for completely attached flow and low drag due to lift at a lift coefficient of $0{\cdot}1$; the corresponding plane wing has also been tested.

The results show that at the design lift both wings have almost the same drag, which is very close to the estimated value for the cambered wing. The good characteristics of the plane wing are due to the facts that at zero C_L the lift-curve slope is underestimated by slender-wing theory, and that at non-zero C_L leading edge separations further increase the lift-curve slope. These increases in lift slope reduce the lift-dependent drag, and this is further reduced by the interaction of the separations on the thickness which produce a favourable axial force.

The flow is attached all over the cambered wing at design, off-design the separations are much weaker than on the plane wing and produce no non-linear lift.

The experimental results on the cambered wing at design lift are not in good agreement with the theoretical values, predicted by slender-wing theory. For example the centre of pressure is $6{\cdot}5\%\ \bar{\bar{c}}$ aft of the predicted position at $M = 1{\cdot}42$, and the lift-curve slope is 40 per cent higher than the slender-wing value, $\pi A/2$, at the same Mach number.

LIST OF SYMBOLS

A	Aspect ratio
$C(y)$	Local chord
c_0	Root chord
$\bar{\bar{c}}$	Mean aerodynamic chord $= \int_{-s}^{s} C^2(y)\,dy \Big/ \int_{-s}^{s} C(y)\,dy$
C_L	Lift coefficient $= L/qS$
C_D	Drag coefficient $= D/qS$
$(C_D)_0$	Drag coefficient of plane wing at zero lift
C_m	Pitching-moment coefficient $= m/qS\bar{\bar{c}}$ (referred to quarter-chord point)
M	Mach number
q	Free stream dynamic pressure
S	Wing area (projected area in plane of uncambered centre section)
s	Semi-span at trailing edge
x, y	Co-ordinate system
α	Wing incidence; incidence of uncambered centre section in cambered wing case
β	$\sqrt{(M^2-1)}$

LIST OF REFERENCES

No.	*Author*	*Title, etc.*
1	W. T. Lord and G. G. Brebner ..	Supersonic flow past narrow wings with 'similar' cross-sections at zero lift. *Aero. Quart.*, Vol. 10, Part 1, February, 1959.
2	J. Weber	Design of warped slender wings with the attachment line along the leading edge. A.R.C. 20051.
3	G. G. Brebner	Some simple conical camber shapes to produce low lift-dependent drag on a slender delta wing. C.P. 428. September, 1957.
4	E. C. Maskell and J. Weber ..	On the aerodynamic design of slender wings. A.R.C. 20610. August, 1958.
5	A. Stanbrook and L. C. Squire ..	Possible types of flow around swept leading edges. Unpublished M.O.A. Report.
6	A. Stanbrook	The lift curve slopes and aerodynamic centre positions of wings at subsonic and supersonic speeds. A.R.C. 17615. November, 1954.
7	Mac. C. Adams and W. R. Sears	Slender body theory—Review and extension. *J. Ae. Sci.*, Vol. 20, February, 1953, p. 85.
8	J. H. B. Smith	The theory of a thin slender conical wing with the wing boundary condition applied at its surface. R. & M. 3135. March, 1958.

TABLE 1

Theoretical properties of the two wings

Plane wing at zero lift

Mach number	1·42	1·61	1·82	2·00
Zero lift wave drag coefficient	0·0082	0·0078	0·0075	0·0072
Turbulent skin-friction drag coefficient (1)	0·0072	0·0069	0·0066	0·0064
Laminar skin-friction drag coefficient (2)	0·0020	0·0020	0·0020	0·0020
C_D:—turbulent	0·0154	0·0147	0·0141	0·0136
C_D:—laminar	0·0102	0·0098	0·0095	0·0092

Cambered wing at design C_L (0·1)

$$C_D = (C_D)_0 + \frac{C_L^2}{\pi A}\left(1{\cdot}07 + \left(\frac{\beta s}{c_0}\right)^2\left\{1{\cdot}88 - 0{\cdot}06\log\frac{\beta s}{c_0}\right\}\right)$$

Mach number	1·42	1·61	1·82	2·00
$(C_D)_0$ turbulent (3)	0·0160	0·0154	0·0147	0·0142
$(C_D)_0$ laminar (3)	0·0104	0·0100	0·0097	0·0095
C_D due to lift	0·0050	0·0054	0·0057	0·0062
L/D at $C_L = 0{\cdot}1$ (turbulent)	4·76	4·81	4·90	4·90
L/D at $C_L = 0{\cdot}1$ (laminar)	6·50	6·50	6·50	6·40

(1) Based on flat plate values—Reynolds number on model mean chord ($1{\cdot}8 \times 10^6$).

(2) Strip theory with no pressure gradients.

(3) The skin-friction drag has been increased for the larger wetted area of the cambered wing.

TABLE 2

Principal dimensions of the models

Plane wing	
Root chord, C_0	20 in.
Span, $2s$	10 in.
Area	133·3 sq. in.
Volume ($0{\cdot}009C_0^3$)	72 cu. in.
$\bar{\bar{c}}$	15 in.
Wetted area	280 sq. in.
Cambered wing	
Root chord	20 in.
Span	10 in.
Area (total area of cambered surface)	145 sq. in.
Volume	72 cu. in.
$\bar{\bar{c}}$	15 in.
Wetted area	305 sq. in.
Dimensions used in coefficients (both wings)	
Area, S	133·3 sq. in.
$\bar{\bar{c}}$	15 in.
Position of quarter-chord point	8·75 in. aft of apex

TABLE 3(a)

Plane wing results (transition fixed)

M	α	C_L	C_m	C_D	M	α	C_L	C_m	C_D
1·42	− 5·09	−0·140	+0·0267	+0·0267	1·82	− 5·25	−0·124	+0·0232	+0·0238
	− 4·10	−0·107	+0·0200	+0·0221		− 4·25	−0·096	+0·0174	+0·0195
	− 3·01	−0·078	+0·0147	+0·0188		− 3·14	−0·068	+0·0120	+0·0166
	− 1·96	−0·046	+0·0083	+0·0167		− 2·09	−0·040	+0·0065	+0·0146
	− 0·93	−0·021	+0·0039	+0·0153		− 1·09	−0·016	+0·0019	+0·0136
	+ 0·11	+0·003	+0·0003	+0·0153		+ 0·01	+0·008	−0·0020	+0·0133
	+ 1·09	+0·027	−0·0036	+0·0158		+ 1·01	+0·032	−0·0061	+0·0142
	+ 2·18	+0·055	−0·0088	+0·0171		+ 2·11	+0·058	−0·0112	+0·0154
	+ 3·17	+0·086	−0·0146	+0·0189		+ 3·12	+0·086	−0·0168	+0·0177
	+ 4·26	+0·116	−0·0203	+0·0226		+ 4·22	+0·114	−0·0225	+0·0212
	+ 5·31	+0·149	−0·0270	+0·0273		+ 5·28	+0·145	−0·0287	+0·0253
	+ 6·35	+0·183	−0·0343	+0·0338		+ 6·29	+0·175	−0·0353	+0·0310
	+ 7·39	+0·217	−0·0410	+0·0410		+ 7·40	+0·207	−0·0422	+0·0383
	+ 8·39	+0·253	−0·0488	+0·0497		+ 8·41	+0·239	−0·0494	+0·0463
	+ 9·43	+0·291	−0·0574	+0·0601		+ 9·47	+0·271	−0·0564	+0·0559
	+10·53	+0·328	−0·0659	+0·0725		+10·52	+0·303	−0·0638	+0·0668
1·61	− 5·13	−0·133	+0·0241	+0·0253	2·00	− 5·22	−0·135	+0·0254	+0·0245
	− 4·17	−0·102	+0·0179	+0·0204		− 4·27	−0·108	+0·0204	+0·0202
	− 3·06	−0·072	+0·0118	+0·0176		− 3·16	−0·080	+0·0150	+0·0167
	− 2·00	−0·045	+0·0067	+0·0152		− 2·11	−0·054	+0·0101	+0·0146
	− 1·00	−0·018	+0·0020	+0·0141		− 1·06	−0·029	+0·0053	+0·0135
	+ 0·10	+0·006	−0·0023	+0·0138		− 0·01	−0·004	+0·0007	+0·0132
	+ 1·11	+0·031	−0·0066	+0·0142		+ 0·99	+0·018	−0·0031	+0·0134
	+ 2·21	+0·058	−0·0117	+0·0156		+ 2·09	+0·042	−0·0078	+0·0144
	+ 3·27	+0·087	−0·0173	+0·0180		+ 3·08	+0·068	−0·0129	+0·0162
	+ 4·27	+0·116	−0·0232	+0·0214		+ 4·18	+0·094	−0·0183	+0·0191
	+ 5·39	+0·148	−0·0298	+0·0264		+ 5·24	+0·122	−0·0243	+0·0233
	+ 6·40	+0·180	−0·0366	+0·0322		+ 6·24	+0·151	−0·0303	+0·0281
	+ 7·46	+0·213	−0·0438	+0·0396		+ 7·34	+0·181	−0·0371	+0·0348
	+ 8·52	+0·248	−0·0515	+0·0484		+ 8·35	+0·210	−0·0430	+0·0419
	+ 9·58	+0·280	−0·0585	+0·0599		+ 9·40	+0·239	−0·0498	+0·0506
	+10·70	+0·315	−0·0666	+0·0705		+10·51	+0·270	−0·0565	+0·0607

TABLE 3(b)

Plane wing results (transition free)

M	α	C_L	C_m	C_D	M	α	C_L	C_m	C_D
1·42	− 5·19	−0·143	+0·0269	+0·0226	1·82	− 5·31	−0·125	+0·0233	+0·0211
	− 4·17	−0·110	+0·0202	+0·0181		− 4·25	−0·098	+0·0186	+0·0169
	− 3·06	−0·079	+0·0143	+0·0147		− 3·14	−0·070	+0·0137	+0·0136
	− 2·00	−0·048	+0·0084	+0·0118		− 2·08	−0·043	+0·0087	+0·0113
	− 0·99	−0·022	+0·0042	+0·0098		− 1·08	−0·017	+0·0039	+0·0095
	+ 0·11	+0·003	−0·0002	+0·0087		+ 0·02	+0·006	−0·0007	+0·0092
	+ 1·12	+0·028	−0·0040	+0·0102		+ 1·02	+0·033	−0·0059	+0·0100
	+ 2·22	+0·055	−0·0084	+0·0121		+ 2·12	+0·058	−0·0109	+0·0117
	+ 3·23	+0·085	−0·0141	+0·0150		+ 3·11	+0·083	−0·0162	+0·0141
	+ 4·30	+0·118	−0·0209	+0·0189		+ 4·17	+0·112	−0·0222	+0·0177
	+ 5·41	+0·151	−0·0273	+0·0240		+ 5·27	+0·141	−0·0282	+0·0222
	+ 6·42	+0·186	−0·0348	+0·0305		+ 6·28	+0·173	−0·0353	+0·0279
	+ 7·54	+0·223	−0·0424	+0·0384		+ 7·39	+0·203	−0·0417	+0·0349
	+ 8·56	+0·259	−0·0503	+0·0473		+ 8·39	+0·235	−0·0487	+0·0429
	+ 9·63	+0·298	−0·0589	+0·0503		+10·56	+0·299	−0·0633	+0·0633
	+10·75	+0·337	−0·0678	+0·0664					
1·61	− 5·23	−0·134	+0·0248	+0·0217	2·00	− 5·20	−0·130	+0·0258	+0·0213
	− 4·11	−0·103	+0·0186	+0·0173		− 4·25	−0·103	+0·0204	+0·0174
	− 3·06	−0·073	+0·0126	+0·0139		− 3·15	−0·075	+0·0148	+0·0139
	− 2·00	−0·043	+0·0068	+0·0113		− 2·10	−0·049	+0·0093	+0·0116
	− 0·99	−0·017	+0·0022	+0·0094		− 1·05	−0·024	+0·0045	+0·0099
	+ 0·11	+0·007	−0·0021	+0·0087		0	0	−0·0002	+0·0094
	+ 2·22	+0·059	−0·0112	+0·0120		+ 0·99	+0·023	−0·0045	+0·0104
	+ 3·27	+0·086	−0·0165	+0·0147		+ 2·09	+0·048	−0·0093	+0·0128
	+ 4·33	+0·117	−0·0227	+0·0184		+ 3·09	+0·072	−0·0141	+0·0134
	+ 5·44	+0·148	−0·0291	+0·0234		+ 4·19	+0·100	−0·0201	+0·0167
	+ 6·45	+0·181	−0·0362	+0·0296		+ 5·24	+0·128	−0·0260	+0·0208
	+ 7·51	+0·215	−0·0437	+0·0370		+ 6·24	+0·156	−0·0319	+0·0260
	+ 8·53	+0·249	−0·0510	+0·0456		+ 7·35	+0·185	−0·0384	+0·0325
	+ 9·59	+0·283	−0·0587	+0·0558		+ 8·35	+0·213	−0·0443	+0·0396
	+10·75	+0·316	−0·0662	+0·0677		+ 9·40	+0·243	−0·0512	+0·0481
						+10·50	+0·271	−0·0575	+0·0580

TABLE 4(a)

Cambered wing results (transition fixed)

M	α	C_L	C_m	C_D	M	α	C_L	C_m	C_D
1·42	− 5·33	−0·209	+0·0458	+0·0471	1·82	− 5·28	−0·180	+0·0388	+0·0413
	− 4·26	−0·177	+0·0387	+0·0396		− 4·27	−0·152	+0·0335	+0·0351
	− 3·15	−0·144	+0·0319	+0·0334		− 3·22	−0·123	+0·0276	+0·0295
	− 2·09	−0·112	+0·0252	+0·0281		− 2·16	−0·095	+0·0219	+0·0256
	− 1·09	−0·082	+0·0190	+0·0256		− 1·11	−0·066	+0·0158	+0·0216
	+ 0·03	−0·049	+0·0121	+0·0234		− 0·05	−0·037	+0·0095	+0·0190
	+ 1·04	−0·017	+0·0057	+0·0191		+ 0·95	−0·009	+0·0035	+0·0174
	+ 2·15	+0·014	−0·0004	+0·0181		+ 2·05	+0·018	−0·0020	+0·0167
	+ 3·21	+0·045	−0·0063	+0·0181		+ 3·05	+0·048	−0·0084	+0·0170
	+ 4·27	+0·075	−0·0119	+0·0194		+ 4·16	+0·078	−0·0147	+0·0185
	+ 5·33	+0·104	−0·0170	+0·0216		+ 5·21	+0·105	−0·0203	+0·0206
	+ 6·39	+0·133	−0·0218	+0·0248		+ 6·36	+0·132	−0·0259	+0·0244
	+ 7·46	+0·162	−0·0263	+0·0290		+ 7·32	+0·160	−0·0315	+0·0283
	+ 8·48	+0·195	−0·0324	+0·0345		+ 8·32	+0·189	−0·0374	+0·0336
	+ 9·60	+0·229	−0·0386	+0·0416		+ 9·38	+0·220	−0·0442	+0·0405
	+10·67	+0·265	−0·0456	+0·0497		+10·49	+0·253	−0·0518	+0·0488
1·61	− 5·26	−0·191	+0·0402	+0·0442	2·00	− 5·32	−0·176	+0·0378	+0·0404
	− 4·25	−0·160	+0·0336	+0·0369		− 4·32	−0·148	+0·0319	+0·0344
	− 3·15	−0·130	+0·0273	+0·0311		− 4·27	−0·148	+0·0318	+0·0340
	− 2·09	−0·101	+0·0211	+0·0266		− 3·22	−0·122	+0·0261	+0·0294
	− 1·08	−0·071	+0·0150	+0·0231		− 2·17	−0·096	+0·0208	+0·0264
	+ 0·03	−0·040	+0·0084	+0·0199		− 1·12	−0·068	+0·0148	+0·0234
	+ 1·03	−0·011	+0·0026	+0·0182		− 0·07	−0·042	+0·0092	+0·0187
	+ 2·14	+0·019	−0·0033	+0·0175		+ 0·98	−0·015	+0·0037	+0·0169
	+ 3·15	+0·048	−0·0092	+0·0178		+ 2·02	+0·010	−0·0016	+0·0162
	+ 4·21	+0·078	−0·0151	+0·0190		+ 3·07	+0·037	−0·0075	+0·0163
	+ 5·31	+0·105	−0·0202	+0·0214		+ 4·12	+0·063	−0·0127	+0·0175
	+ 6·32	+0·134	−0·0254	+0·0246		+ 5·17	+0·090	−0·0184	+0·0197
	+ 7·43	+0·163	−0·0308	+0·0293		+ 6·22	+0·116	−0·0234	+0·0229
	+ 8·45	+0·193	−0·0364	+0·0345		+ 7·27	+0·142	−0·0287	+0·0268
	+ 9·56	+0·225	−0·0429	+0·0416		+ 8·28	+0·170	−0·0343	+0·0317
	+10·63	+0·259	−0·0500	+0·0498		+ 9·38	+0·198	−0·0398	+0·0382
						+10·44	+0·227	−0·0462	+0·0454

TABLE 4(b)

Cambered wing results (transition free)

M	α	C_L	C_m	C_D	M	α	C_L	C_m	C_D
1·42	− 5·28	−0·211	+0·0464	+0·0426	1·82	− 5·33	−0·181	+0·0396	+0·0374
	− 4·26	−0·179	+0·0394	+0·0351		− 4·33	−0·153	+0·0333	+0·0312
	− 3·15	−0·146	+0·0323	+0·0292		− 3·22	−0·125	+0·0273	+0·0259
	− 2·09	−0·112	+0·0254	+0·0243		− 2·17	−0·096	+0·0212	+0·0217
	− 1·03	−0·081	+0·0192	+0·0203		− 1·12	−0·067	+0·0151	+0·0183
	+ 0·03	−0·048	+0·0124	+0·0174		− 0·06	−0·039	+0·0091	+0·0159
	+ 1·04	−0·015	+0·0059	+0·0154		+ 0·99	−0·010	+0·0028	+0·0142
	+ 2·15	+0·015	−0·0002	+0·0143		+ 2·04	+0·019	−0·0033	+0·0135
	+ 3·21	+0·047	−0·0069	+0·0144		+ 3·04	+0·047	−0·0091	+0·0136
	+ 4·27	+0·078	−0·0131	+0·0148		+ 4·14	+0·074	−0·0146	+0·0147
	+ 5·33	+0·108	−0·0188	+0·0166		+ 5·20	+0·103	−0·0210	+0·0165
	+ 6·34	+0·137	−0·0231	+0·0199		+ 6·25	+0·130	−0·0267	+0·0196
	+ 7·41	+0·163	−0·0267	+0·0249		+ 7·35	+0·157	−0·0319	+0·0243
	+ 8·48	+0·196	−0·0327	+0·0308		+ 8·36	+0·186	−0·0374	+0·0299
	+ 9·60	+0·230	−0·0389	+0·0379		+ 9·37	+0·218	−0·0439	+0·0366
	+10·62	+0·267	−0·0460	+0·0461		+10·48	+0·249	−0·0507	+0·0448
1·61	− 5·29	−0·186	+0·0403	+0·0389	2·00	− 5·27	−0·177	+0·0382	+0·0370
	− 4·24	−0·156	+0·0329	+0·0319		− 4·27	−0·148	+0·0318	+0·0312
	− 3·14	−0·127	+0·0260	+0·0263		− 3·22	−0·122	+0·0265	+0·0260
	− 2·09	−0·097	+0·0199	+0·0221		− 2·17	−0·096	+0·0211	+0·0220
	− 1·08	−0·068	+0·0139	+0·0190		− 1·17	−0·070	+0·0156	+0·0184
	+ 0·03	−0·038	+0·0078	+0·0163		− 0·07	−0·042	+0·0099	+0·0158
	+ 1·04	−0·008	+0·0016	+0·0147		+ 0·93	−0·016	+0·0044	+0·0141
	+ 2·09	+0·022	−0·0043	+0·0141		+ 1·98	+0·012	−0·0013	+0·0135
	+ 3·20	+0·051	−0·0102	+0·0142		+ 3·08	+0·038	−0·0068	+0·0137
	+ 4·26	+0·081	−0·0162	+0·0150		+ 4·13	+0·066	−0·0128	+0·0148
	+ 5·31	+0·110	−0·0219	+0·0171		+ 5·18	+0·092	−0·0182	+0·0167
	+ 6·32	+0·138	−0·0270	+0·0203		+ 6·23	+0·119	−0·0240	+0·0196
	+ 7·43	+0·166	−0·0319	+0·0252		+ 7·28	+0·147	−0·0297	+0·0235
	+ 8·45	+0·196	−0·0375	+0·0310		+ 8·29	+0·174	−0·0351	+0·0290
	+ 9·56	+0·228	−0·0439	+0·0382		+ 9·34	+0·202	−0·0406	+0·0352
	+10·63	+0·263	−0·0511	+0·0465		+10·45	+0·232	−0·0467	+0·0430

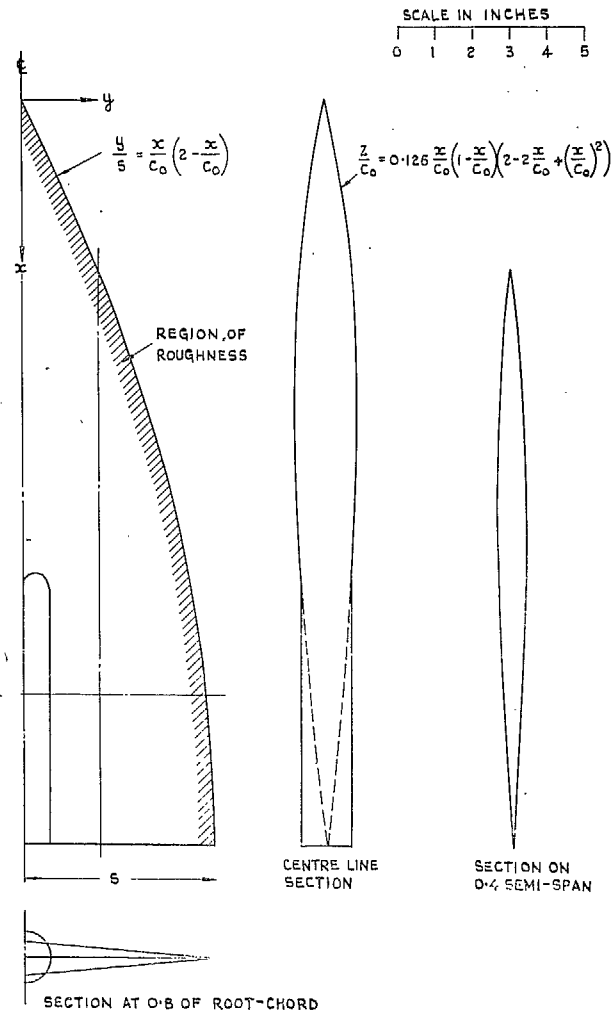

FIG. 1. Details of plane wing.

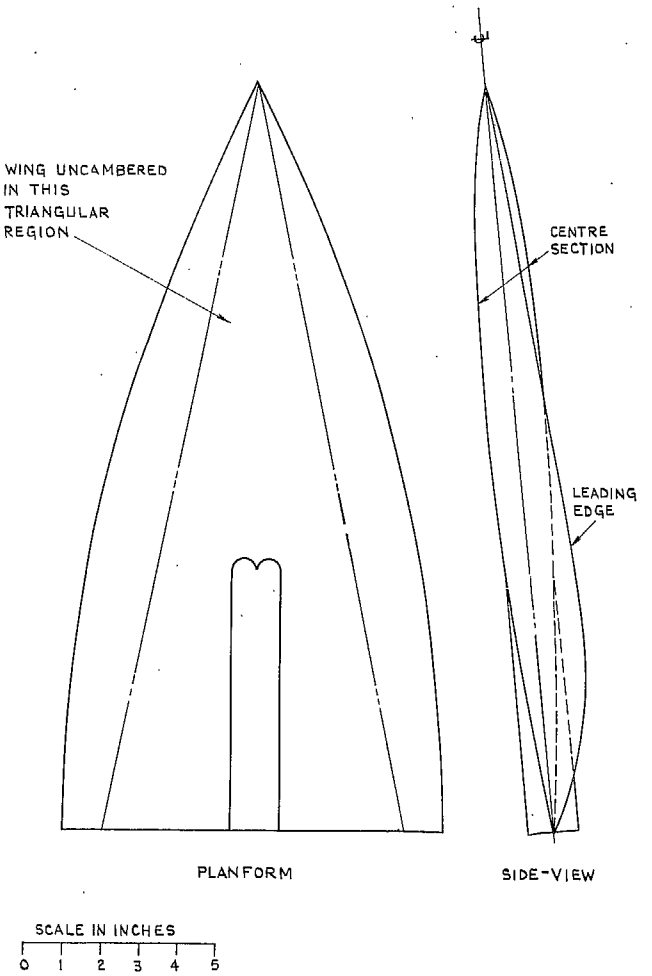

FIG. 2. Details of the cambered wing.

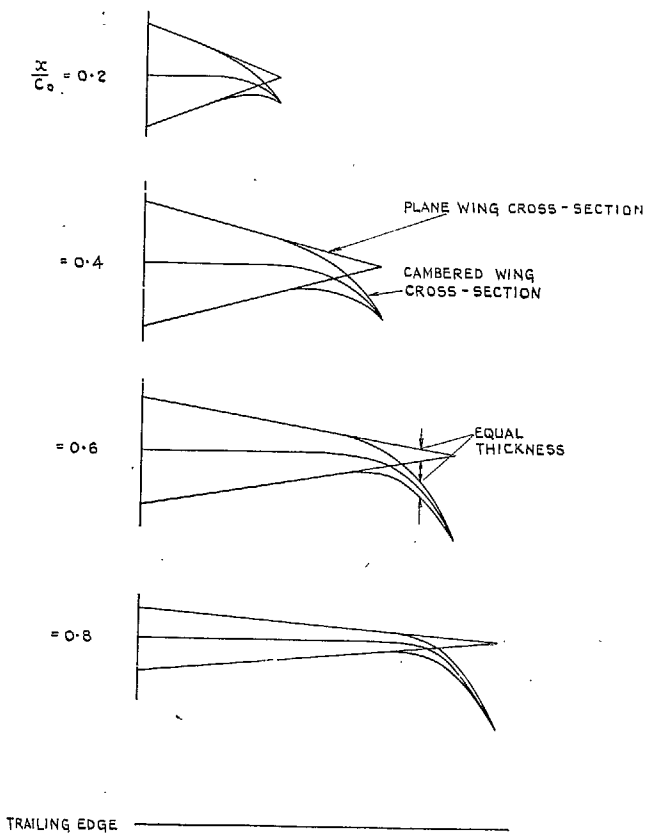

FIG. 3. Details of cambered wing sections.

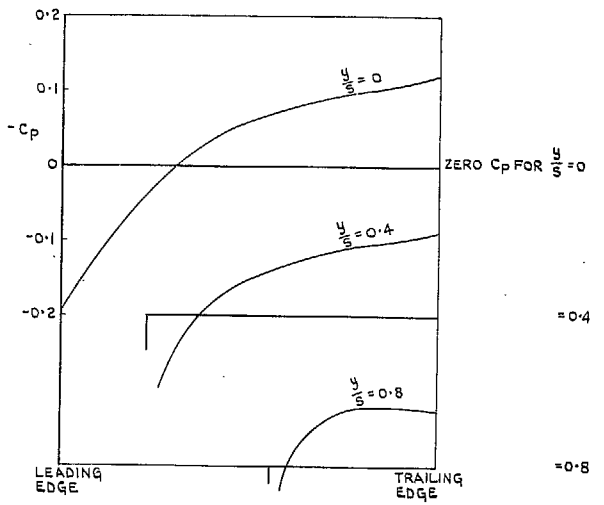

FIG. 4. Theoretical pressure distribution on the plane wing (zero incidence).

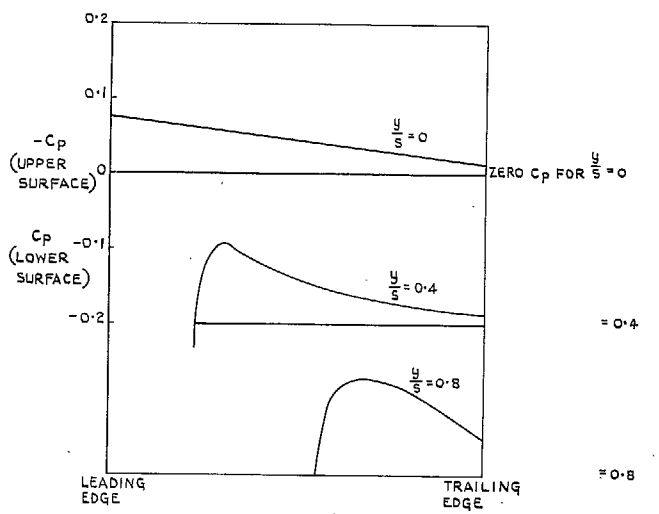

FIG. 5. Theoretical pressure distributions on the thin cambered wing (design C_L).

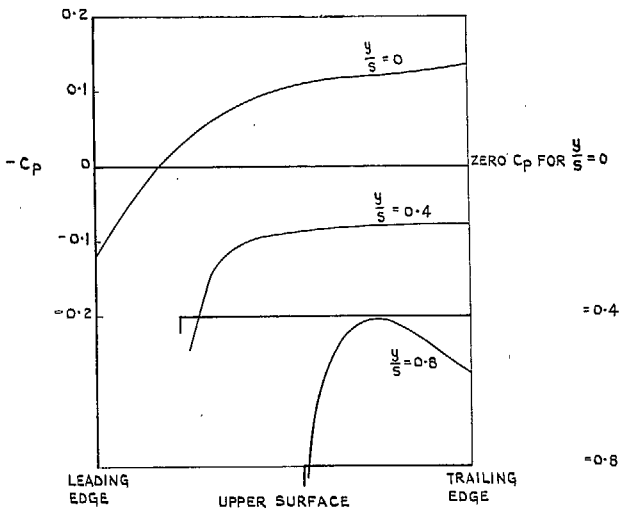

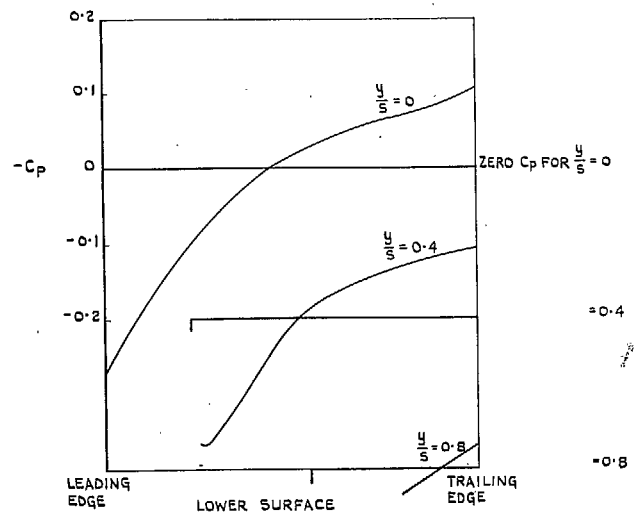

FIG. 6. Theoretical pressure distributions on the thick cambered wing (design C_L).

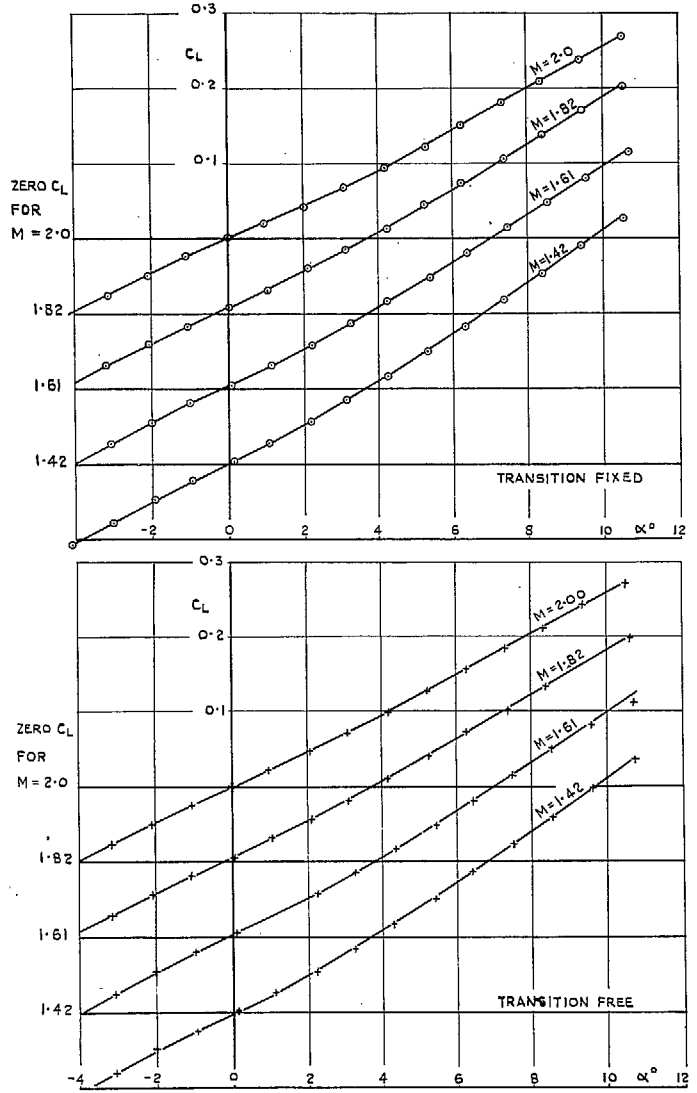

FIG. 7. Variation of C_L with α. Plane wing.

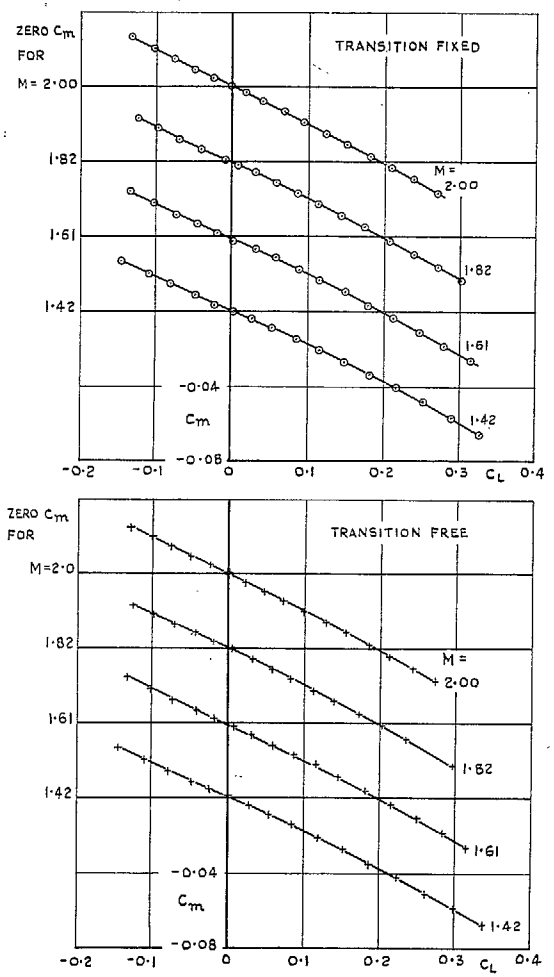

FIG. 8. Variation of C_m with C_L. Plane wing.

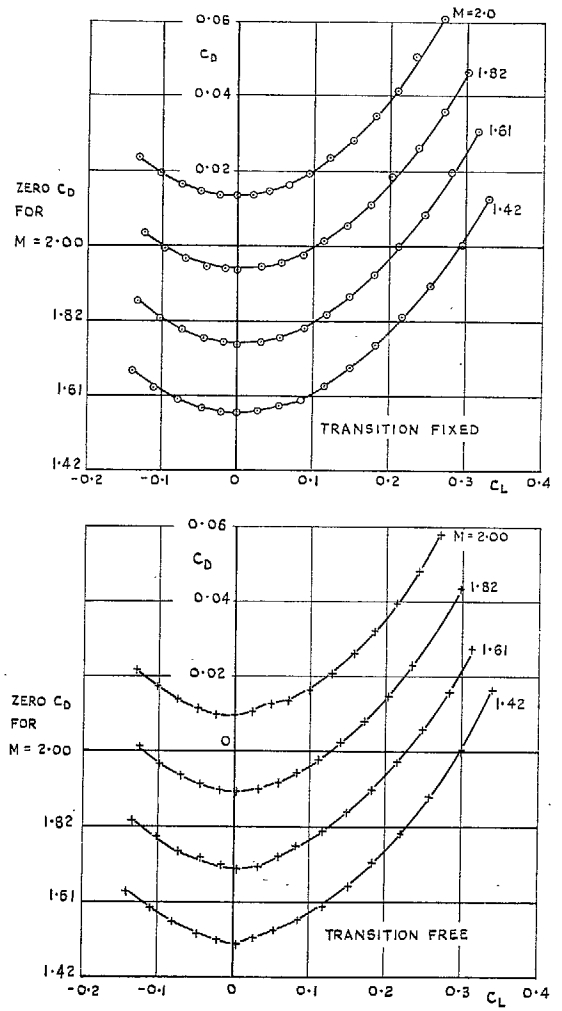

FIG. 9. Variation of C_D with C_L. Plane wing.

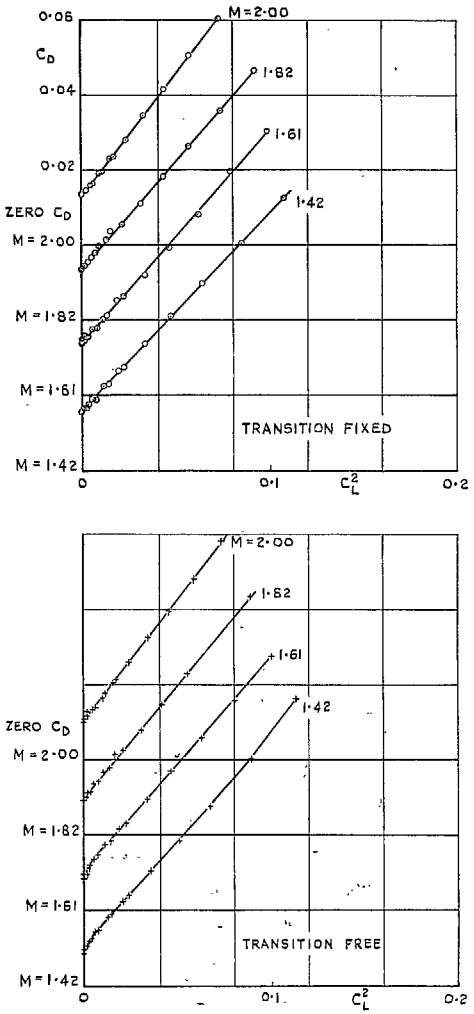

FIG. 10. Variation of C_D with $C_L{}^2$. Plane wing.

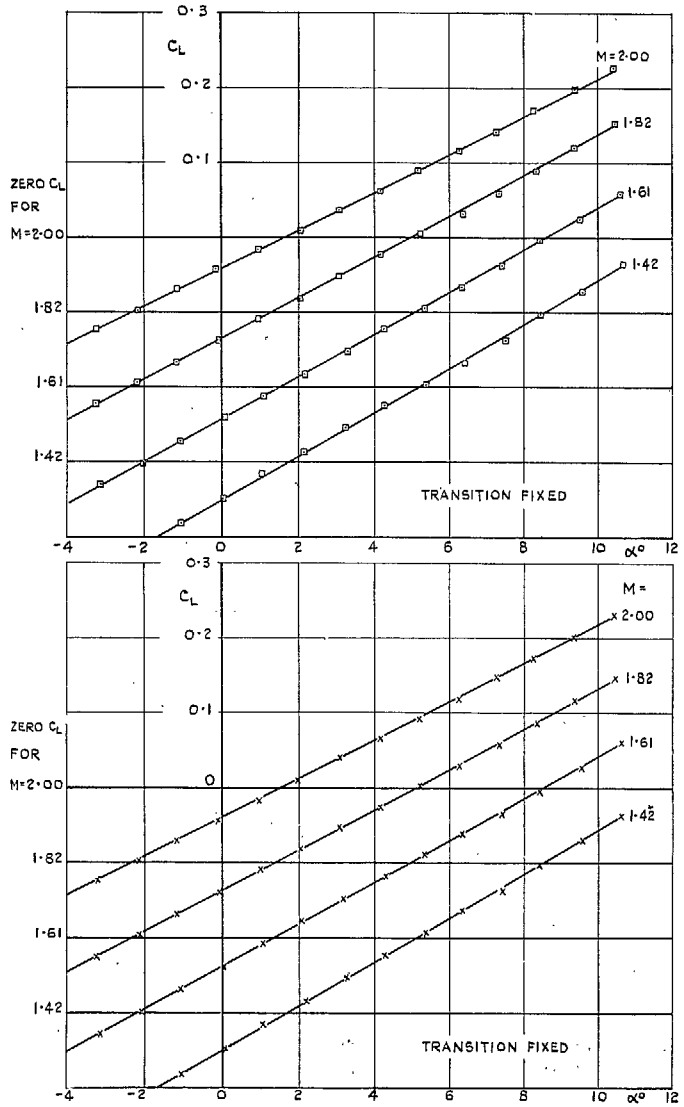

FIG. 11. Variation of C_L with α. Cambered wing.

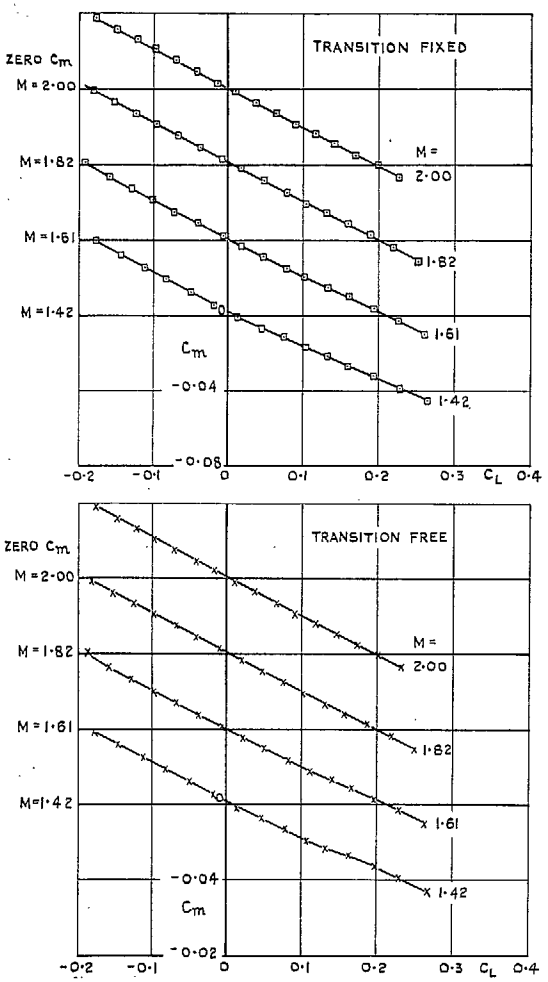

FIG. 12. Variation of C_m with C_L. Cambered wing.

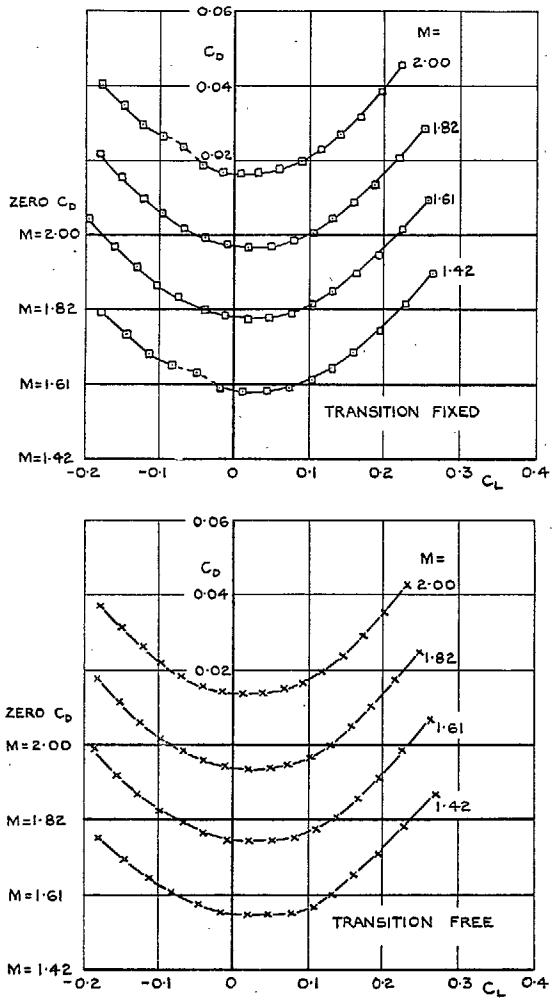

FIG. 13. Variation of C_D with C_L. Cambered wing.

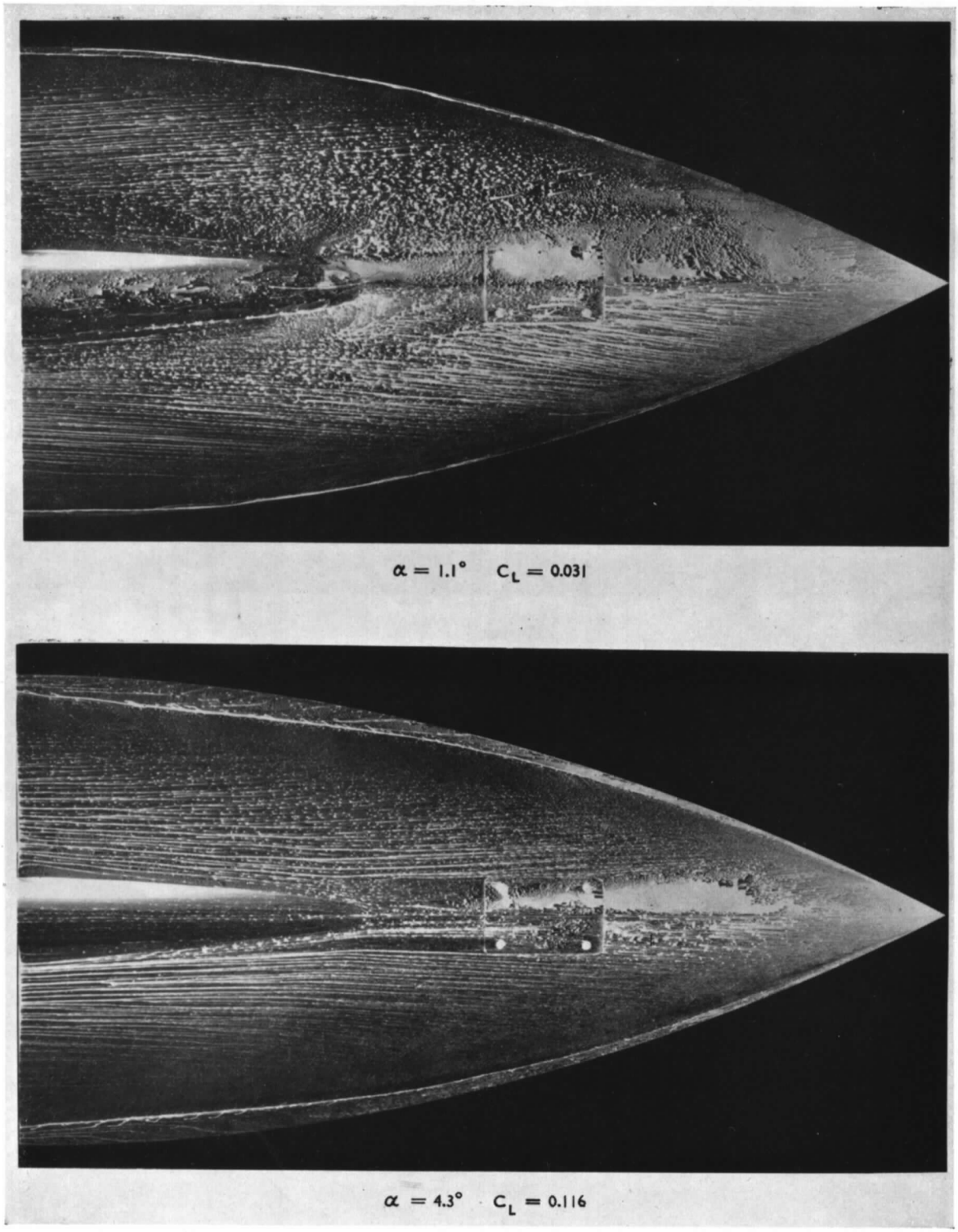

FIG. 14. Oil flow patterns on the plane wing suction surface: $M = 1{\cdot}61$.

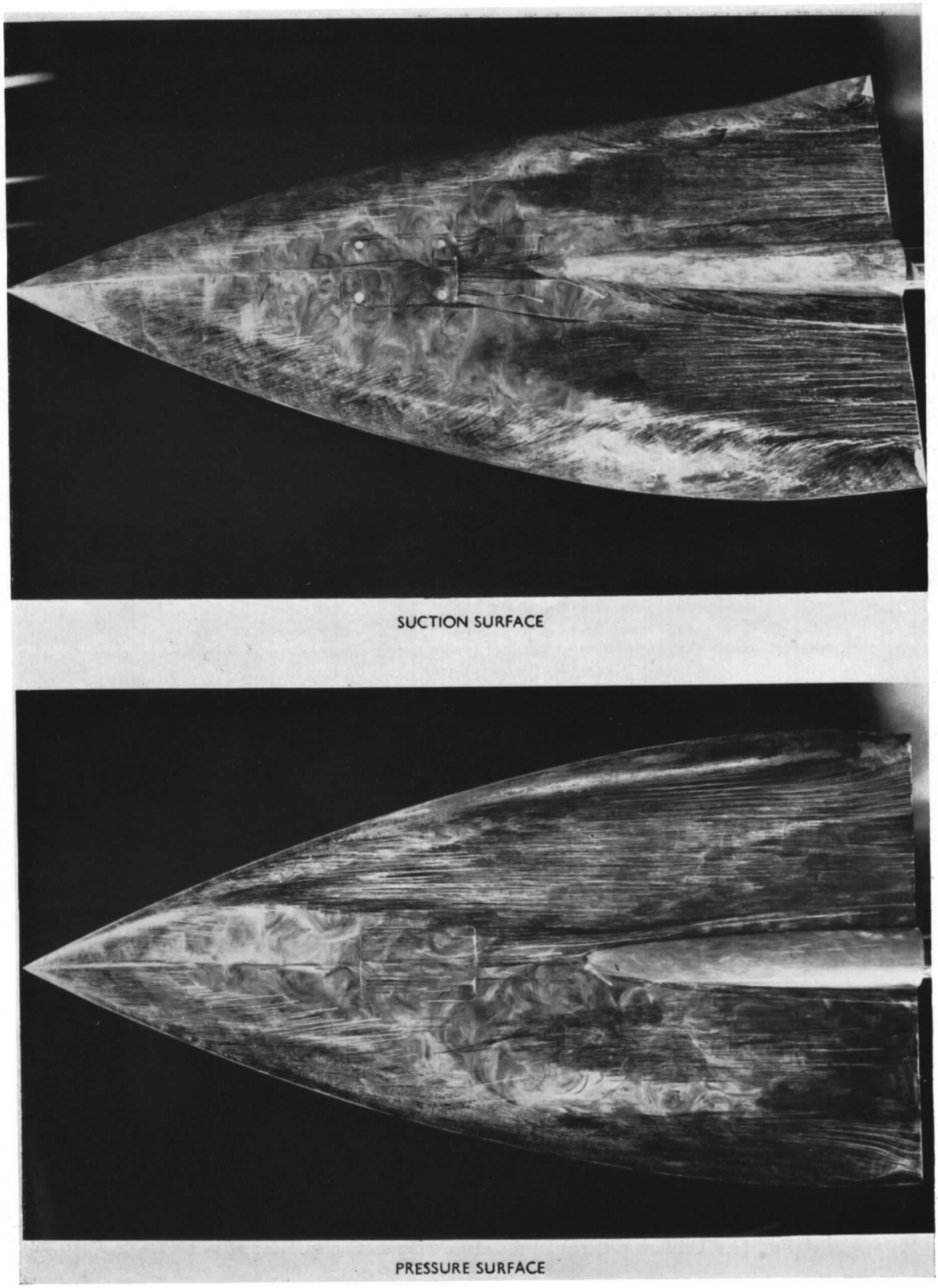

FIG. 15. Oil flow patterns on the cambered wing at design lift coefficient ($C_L = 0{\cdot}1 \quad M = 1{\cdot}61$).

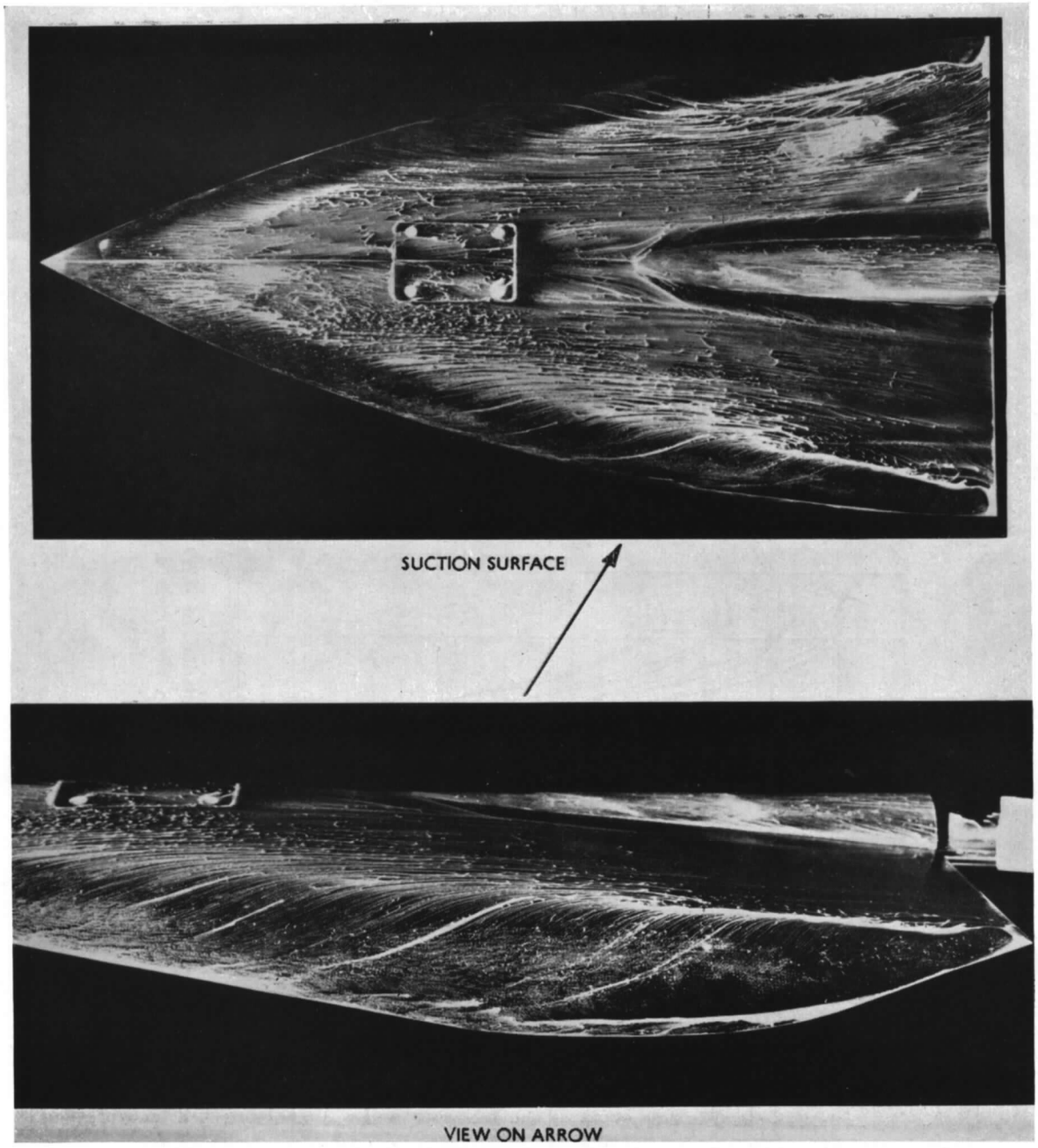

FIG. 16. Oil flow patterns on the cambered wing at $C_L = 0{\cdot}198$ $(M = 1{\cdot}61)$.

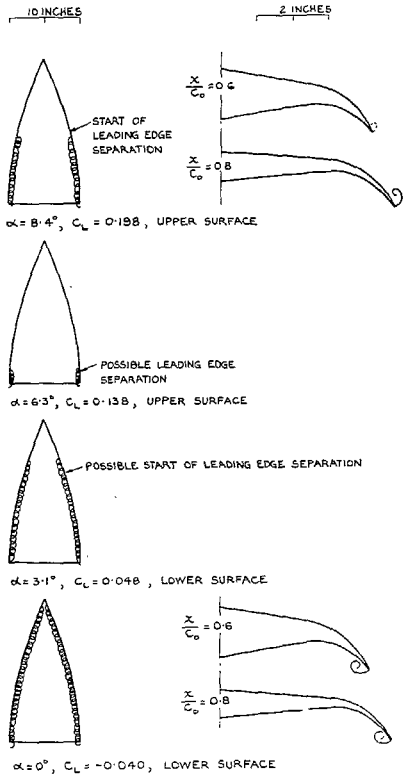

FIG. 17. Vortex positions on the cambered wing. $M = 1{\cdot}61$.

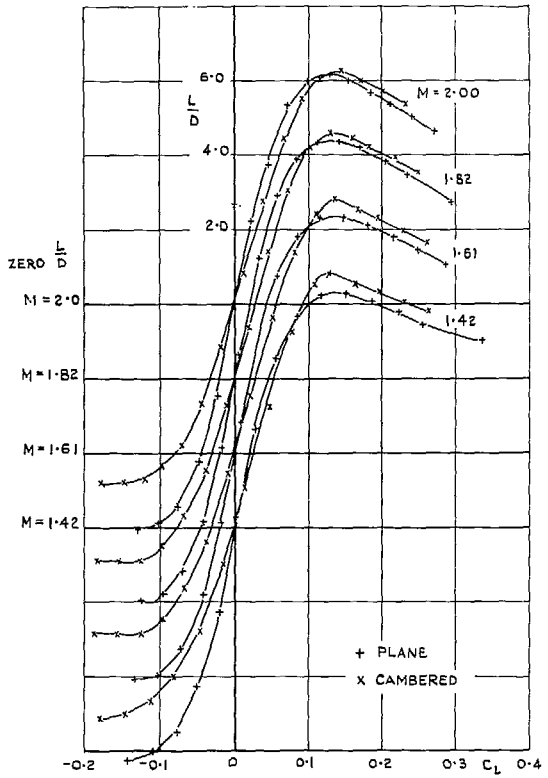

FIG. 18. Variation of L/D with C_L. Cambered and plane wings. Transition free.

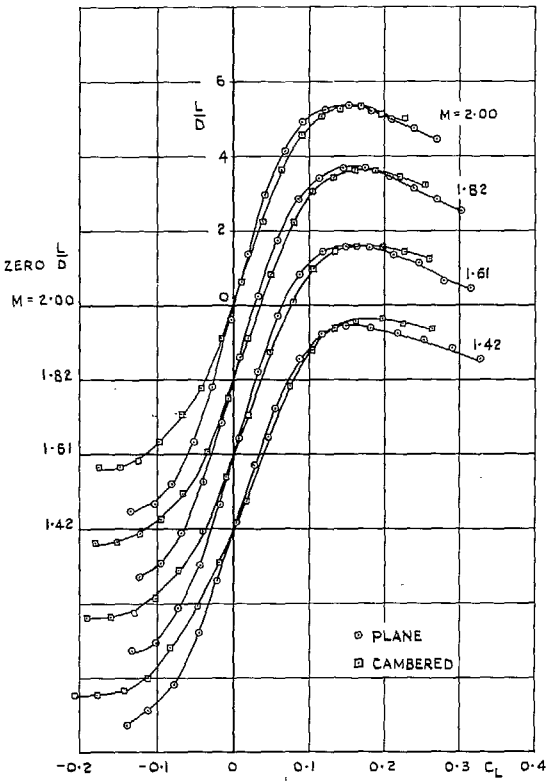

FIG. 19. Variation of L/D with C_L. Cambered and plane wings. Transition fixed.

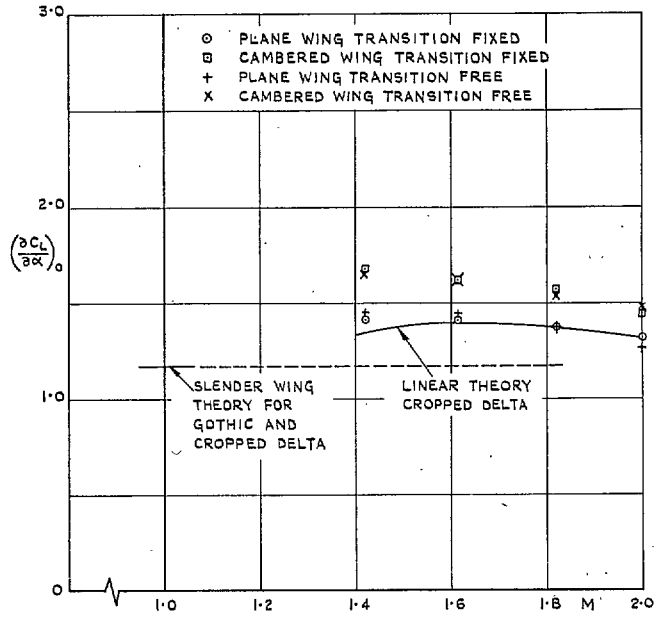

FIG. 20. Variation with Mach number of $(\partial C_L/\partial \alpha)_0$.

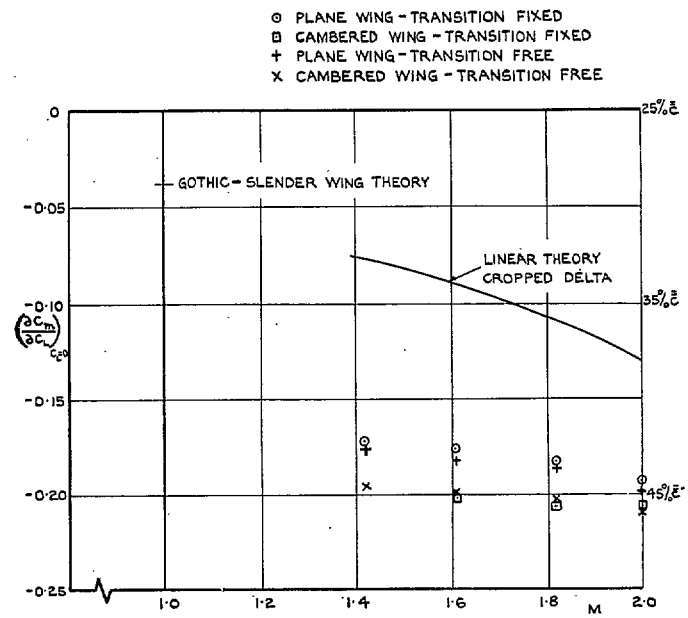

FIG. 21. Variation with Mach number of $(\partial C_m/\partial C_L)_{C_L=0}$.

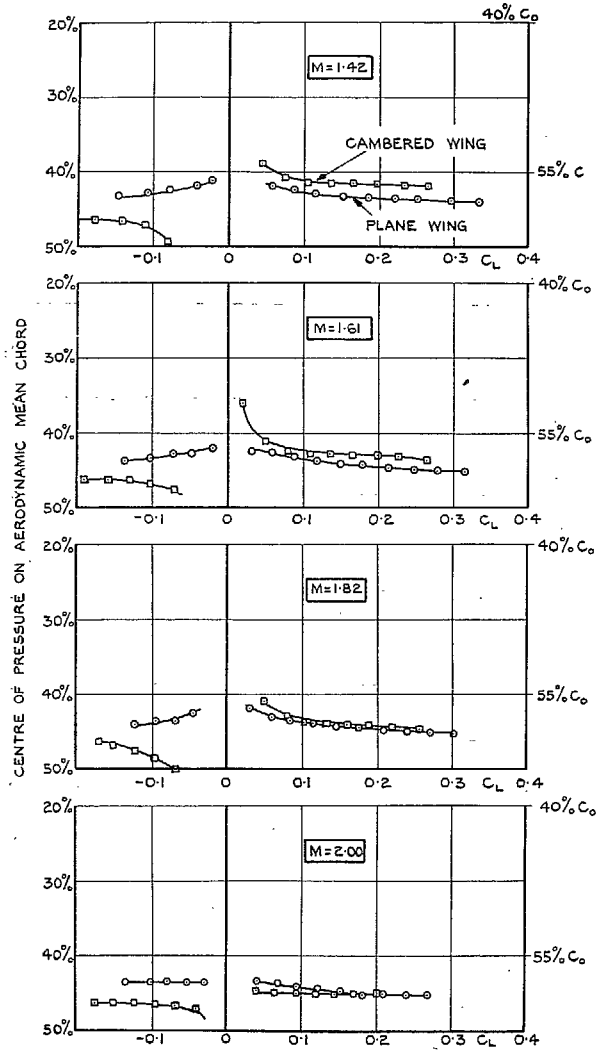

FIG. 22. Variation of centre of pressure with C_L. Cambered and plane wings. Transition fixed.

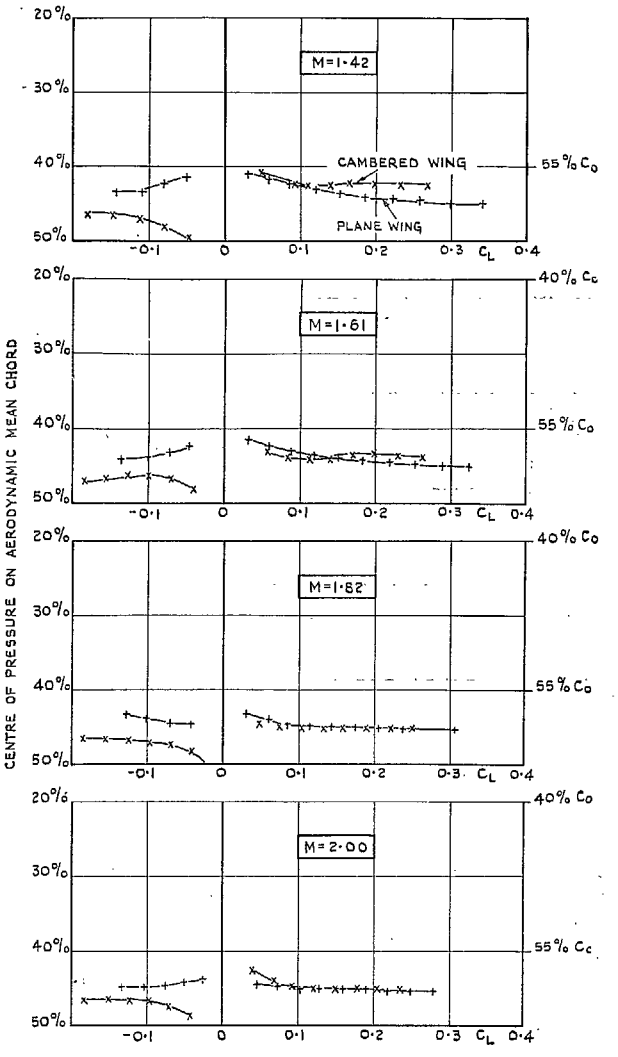

FIG. 23. Variation of centre of pressure with C_L. Cambered and plane wings. Transition free.

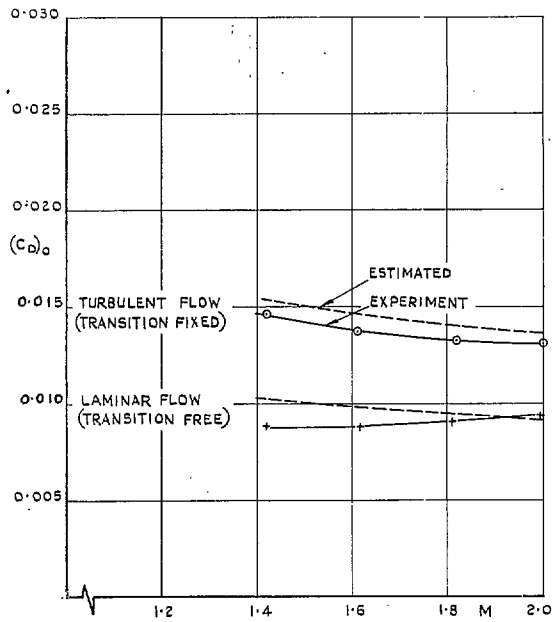

FIG. 24. Variation with Mach number of zero-lift drag of the plane wing.

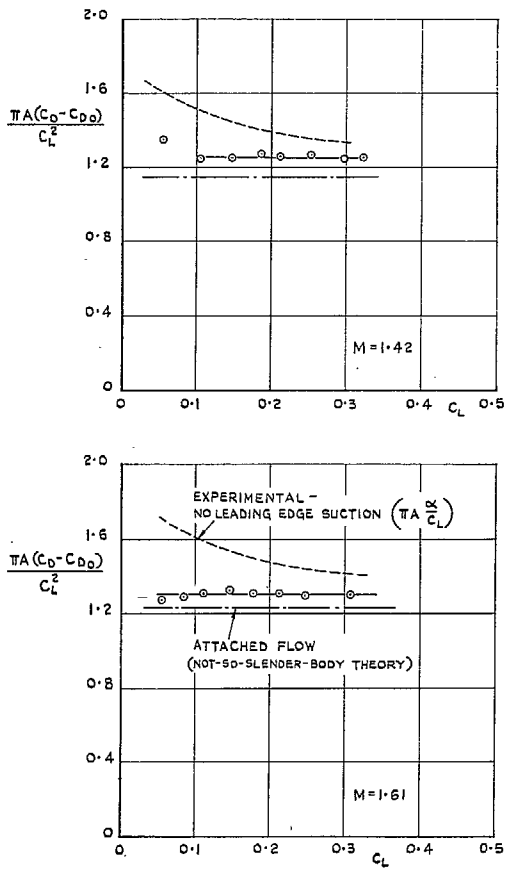

FIG. 25(a). Variation with C_L of the lift-dependent drag factor of the plane wing. $M = 1{\cdot}42$, $1{\cdot}61$.

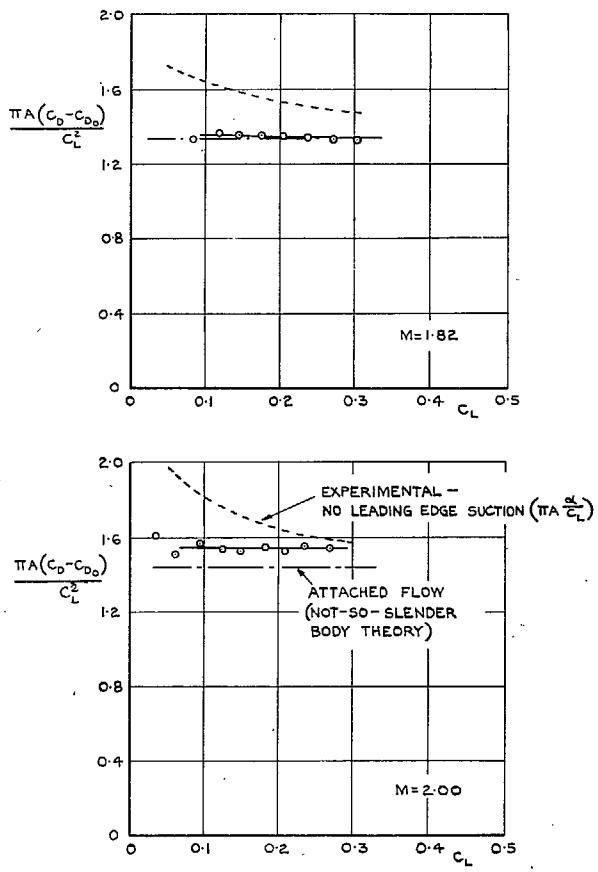

FIG. 25(b). Variation with C_L of the lift-dependent drag factor of the plane wing. $M = 1{\cdot}82$, $2{\cdot}00$.

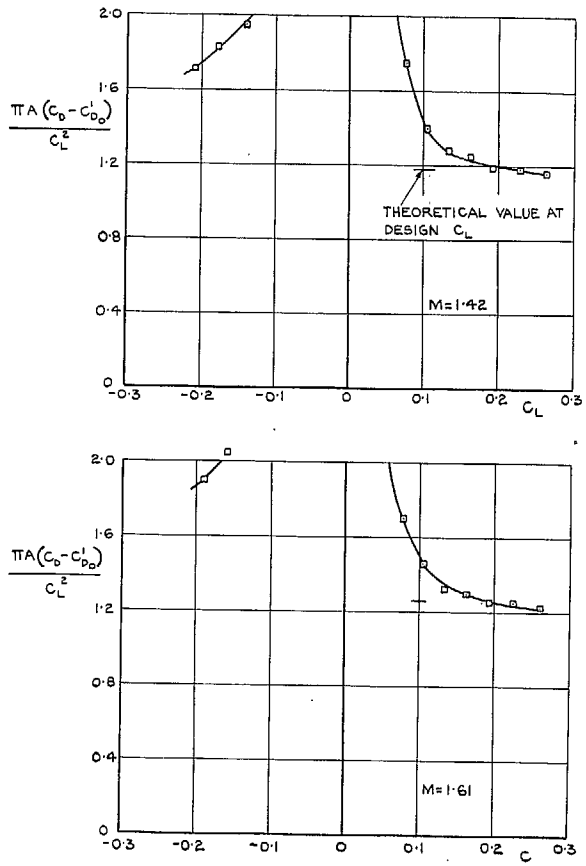

FIG. 26(a). Variation with C_L of the lift-dependent drag factor of the cambered wing. $M = 1{\cdot}42, 1{\cdot}61$.

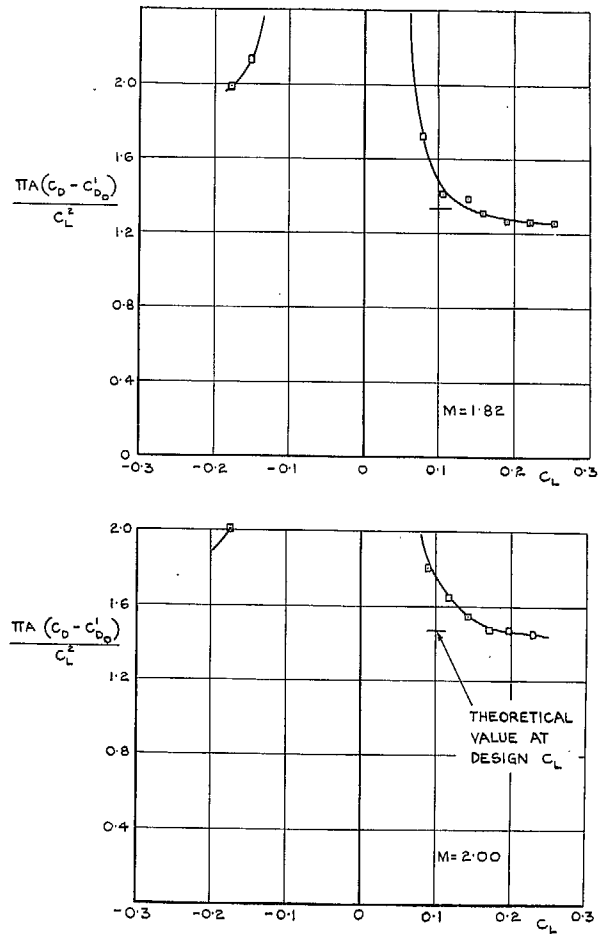

FIG. 26(b). Variation with C_L of the lift-dependent drag factor of the cambered wing. $M = 1{\cdot}82, 2{\cdot}00$.

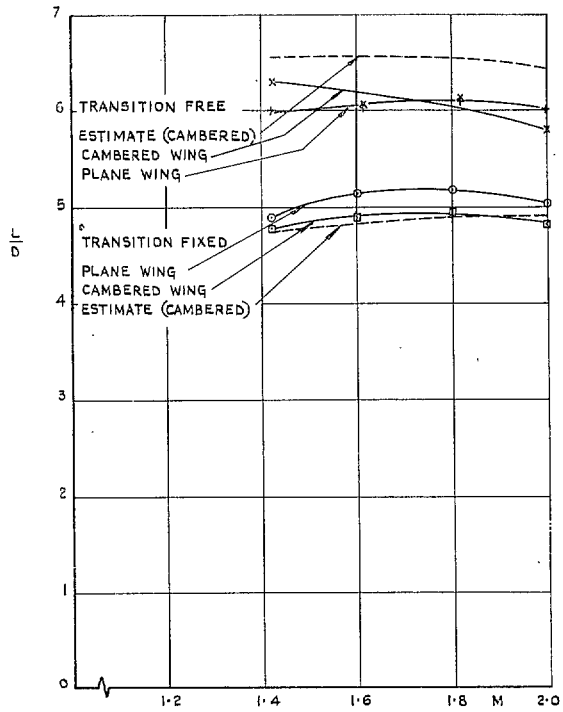

FIG. 27. Variation with Mach number of L/D at $C_L = 0{\cdot}1$.

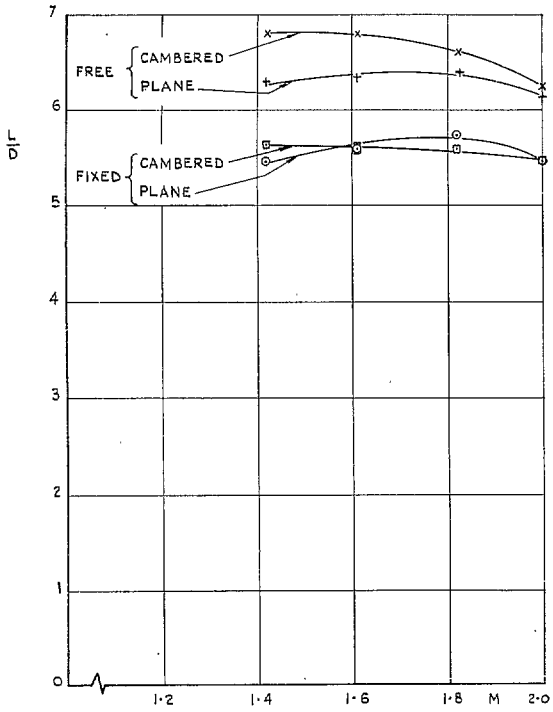

FIG. 28. Variation with Mach number of maximum L/D.

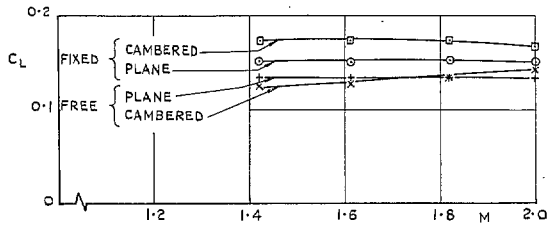

FIG. 29. Variation with Mach number of C_L for maximum L/D.

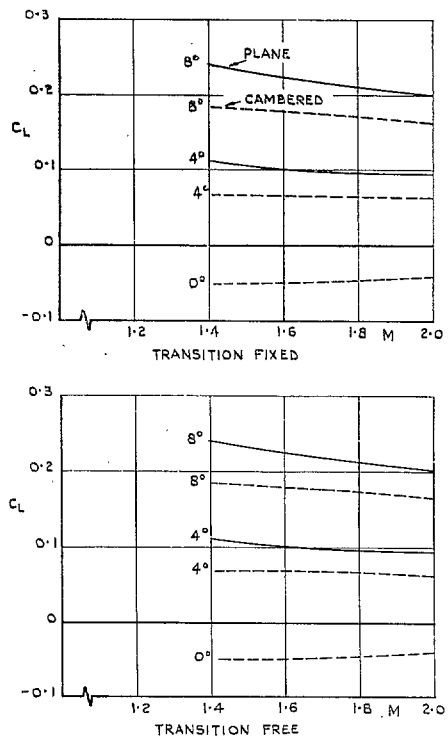

FIG. 30. Variation with Mach number of C_L at fixed incidence. Cambered and plane wings.

(82029) Wt. 66/991 K.5 7/61 Hw.

R. & M. No. 3211

533.6.011.5:
533.693.3:
533.6.013.12

AN EXPERIMENTAL INVESTIGATION AT SUPERSONIC SPEEDS OF THE CHARACTERISTICS OF TWO GOTHIC WINGS, ONE PLANE AND ONE CAMBERED. L. C. Squire
May, 1959

Tests have been made at supersonic speeds up to $M = 2{\cdot}0$ on a thick cambered gothic wing of aspect ratio $0{\cdot}75$, together with tests on the uncambered wing of the same planform and thickness. The camber was designed to give attached flow all along the leading edge, and over the

P.T.O.

R. & M. No. 3211

533.6.011.5:
533.693.3:
533.6.013.12

AN EXPERIMENTAL INVESTIGATION AT SUPERSONIC SPEEDS OF THE CHARACTERISTICS OF TWO GOTHIC WINGS, ONE PLANE AND ONE CAMBERED. L. C. Squire
May, 1959

Tests have been made at supersonic speeds up to $M = 2{\cdot}0$ on a thick cambered gothic wing of aspect ratio $0{\cdot}75$, together with tests on the uncambered wing of the same planform and thickness. The camber was designed to give attached flow all along the leading edge, and over the

P.T.O.

R. & M. No. 3211

533.6.011.5:
533.693.3:
533.6.013.12

AN EXPERIMENTAL INVESTIGATION AT SUPERSONIC SPEEDS OF THE CHARACTERISTICS OF TWO GOTHIC WINGS, ONE PLANE AND ONE CAMBERED. L. C. Squire
May, 1959

Tests have been made at supersonic speeds up to $M = 2{\cdot}0$ on a thick cambered gothic wing of aspect ratio $0{\cdot}75$, together with tests on the uncambered wing of the same planform and thickness. The camber was designed to give attached flow all along the leading edge, and over the

P.T.O.

R. & M. No. 3211

533.6.011.5:
533.693.3:
533.6.013.12

AN EXPERIMENTAL INVESTIGATION AT SUPERSONIC SPEEDS OF THE CHARACTERISTICS OF TWO GOTHIC WINGS, ONE PLANE AND ONE CAMBERED. L. C. Squire
May, 1959

Tests have been made at supersonic speeds up to $M = 2{\cdot}0$ on a thick cambered gothic wing of aspect ratio $0{\cdot}75$, together with tests on the uncambered wing of the same planform and thickness. The camber was designed to give attached flow all along the leading edge, and over the

P.T.O.

whole wing, at one lift coefficient, together with low drag at this lift. The thickness distribution was chosen to have low zero lift drag and also to eliminate the adverse pressure gradients due to incidence and camber at the design lift.

The results show that the drag of the cambered wing is close to the theoretically estimated value at the design lift coefficient; the drag of the plane wing, however, is also of the same magnitude and the reasons for this are discussed. Other properties of the wings are not in agreement with the slender thin wing theory. At the design condition on the cambered wing the flow is attached over the whole wing. Off the design condition the leading edge separations on the cambered wing are much weaker than on the plane wing.

whole wing, at one lift coefficient, together with low drag at this lift. The thickness distribution was chosen to have low zero lift drag and also to eliminate the adverse pressure gradients due to incidence and camber at the design lift.

The results show that the drag of the cambered wing is close to the theoretically estimated value at the design lift coefficient; the drag of the plane wing, however, is also of the same magnitude and the reasons for this are discussed. Other properties of the wings are not in agreement with the slender thin wing theory. At the design condition on the cambered wing the flow is attached over the whole wing. Off the design condition the leading edge separations on the cambered wing are much weaker than on the plane wing.

whole wing, at one lift coefficient, together with low drag at this lift. The thickness distribution was chosen to have low zero lift drag and also to eliminate the adverse pressure gradients due to incidence and camber at the design lift.

The results show that the drag of the cambered wing is close to the theoretically estimated value at the design lift coefficient; the drag of the plane wing, however, is also of the same magnitude and the reasons for this are discussed. Other properties of the wings are not in agreement with the slender thin wing theory. At the design condition on the cambered wing the flow is attached over the whole wing. Off the design condition the leading edge separations on the cambered wing are much weaker than on the plane wing.

whole wing, at one lift coefficient, together with low drag at this lift. The thickness distribution was chosen to have low zero lift drag and also to eliminate the adverse pressure gradients due to incidence and camber at the design lift.

The results show that the drag of the cambered wing is close to the theoretically estimated value at the design lift coefficient; the drag of the plane wing, however, is also of the same magnitude and the reasons for this are discussed. Other properties of the wings are not in agreement with the slender thin wing theory. At the design condition on the cambered wing the flow is attached over the whole wing. Off the design condition the leading edge separations on the cambered wing are much weaker than on the plane wing.

Publications of the Aeronautical Research Council

ANNUAL TECHNICAL REPORTS OF THE AERONAUTICAL RESEARCH COUNCIL (BOUND VOLUMES)

1941 Aero and Hydrodynamics, Aerofoils, Airscrews, Engines, Flutter, Stability and Control, Structures. 63*s.* (post 2*s.* 3*d.*)

1942 Vol. I. Aero and Hydrodynamics, Aerofoils, Airscrews, Engines. 75*s.* (post 2*s.* 3*d.*)
Vol. II. Noise, Parachutes, Stability and Control, Structures, Vibration, Wind Tunnels. 47*s.* 6*d.* (post 1*s.* 9*d.*)

1943 Vol. I. Aerodynamics, Aerofoils, Airscrews. 80*s.* (post 2*s.*)
Vol. II. Engines, Flutter, Materials, Parachutes, Performance, Stability and Control, Structures. 90*s.* (post 2*s.* 3*d.*)

1944 Vol. I. Aero and Hydrodynamics, Aerofoils, Aircraft, Airscrews, Controls. 84*s.* (post 2*s.* 6*d.*)
Vol. II. Flutter and Vibration, Materials, Miscellaneous, Navigation, Parachutes, Performance, Plates and Panels, Stability, Structures, Test Equipment, Wind Tunnels. 84*s.* (post 2*s.* 6*d.*)

1945 Vol. I. Aero and Hydrodynamics, Aerofoils. 130*s.* (post 3*s.*)
Vol. II. Aircraft, Airscrews, Controls. 130*s.* (post 3*s.*)
Vol. III. Flutter and Vibration, Instruments, Miscellaneous, Parachutes, Plates and Panels, Propulsion. 130*s.* (post 2*s.* 9*d.*)
Vol. IV. Stability, Structures, Wind Tunnels, Wind Tunnel Technique. 130*s.* (post 2*s.* 9*d.*)

1946 Vol. I. Accidents, Aerodynamics, Aerofoils and Hydrofoils. 168*s.* (post 3*s.* 3*d.*)
Vol. II. Airscrews, Cabin Cooling, Chemical Hazards, Controls, Flames, Flutter, Helicopters, Instruments and Instrumentation, Interference, Jets, Miscellaneous, Parachutes. 168s. (post 2*s.* 9*d.*)
Vol. III. Performance, Propulsion, Seaplanes, Stability, Structures, Wind Tunnels. 168*s.* (post 3*s.*)

1947 Vol. I. Aerodynamics, Aerofoils, Aircraft. 168*s.* (post 3*s.* 3*d.*)
Vol. II. Airscrews and Rotors, Controls, Flutter, Materials, Miscellaneous, Parachutes, Propulsion, Seaplanes, Stability, Structures, Take-off and Landing. 168*s.* (post 3*s.* 3*d.*)

Special Volumes

Vol. I. Aero and Hydrodynamics, Aerofoils, Controls, Flutter, Kites, Parachutes, Performance, Propulsion, Stability. 126*s.* (post 2*s.* 6*d.*)
Vol. II. Aero and Hydrodynamics, Aerofoils, Airscrews, Controls, Flutter, Materials, Miscellaneous, Parachutes, Propulsion, Stability, Structures. 147*s.* (post 2*s.* 6*d.*)
Vol. III. Aero and Hydrodynamics, Aerofoils, Airscrews, Controls, Flutter, Kites, Miscellaneous, Parachutes, Propulsion, Seaplanes, Stability, Structures, Test Equipment. 189*s.* (post 3*s.* 3*d.*)

Reviews of the Aeronautical Research Council

1939–48 3*s.* (post 5*d.*) 1949–54 5*s.* (post 5*d.*)

Index to all Reports and Memoranda published in the Annual Technical Reports

1909–1947 R. & M. 2600 6*s.* (post 2*d.*)

Indexes to the Reports and Memoranda of the Aeronautical Research Council

Between Nos. 2351–2449	R. & M. No. 2450 2*s.* (post 2*d.*)
Between Nos. 2451–2549	R. & M. No. 2550 2*s.* 6*d.* (post 2*d.*)
Between Nos. 2551–2649	R. & M. No. 2650 2*s.* 6*d.* (post 2*d.*)
Between Nos. 2651–2749	R. & M. No. 2750 2*s.* 6*d.* (post 2*d.*)
Between Nos. 2751–2849	R. & M. No. 2850 2*s.* 6*d.* (post 2*d.*)
Between Nos. 2851–2949	R. & M. No. 2950 3*s.* (post 2*d.*)
Between Nos. 2951–3049	R. & M. No. 3050 3*s.* 6*d.* (post 2*d.*)

HER MAJESTY'S STATIONERY OFFICE

from the addresses overleaf

Printed and published by
HER MAJESTY'S STATIONERY OFFICE

To be purchased from
York House, Kingsway, London W.C.2
423 Oxford Street, London W.1
13A Castle Street, Edinburgh 2
109 St. Mary Street, Cardiff
39 King Street, Manchester 2
50 Fairfax Street, Bristol 1
2 Edmund Street, Birmingham 3
80 Chichester Street, Belfast 1
or through any bookseller

Printed in England

S.O. Code No. 23-3211